Elsevier Editorial System(tm) for Lithos
Manuscript Draft

Manuscript Number:

Title: Eocene-Miocene igneous activity in Provence (SE France): 40Ar/39Ar data, geochemical-petrological constraints and geodynamic implications

Article Type: Regular Article

Keywords: Provence, petrology, Mediterranean, geodynamics, subduction, 40Ar/39Ar geochronology, Sr-Nd-Pb systematic

Corresponding Author: Professor Michele Lustrino, PhD

Corresponding Author's Institution: Università degli Studi di Roma La Sapienza

First Author: Michele Lustrino, PhD

Order of Authors: Michele Lustrino, PhD; Lorenzo Fedele, PhD; Samuele Agostini, PhD; Gianfranco Di Vincenzo, PhD; Vincenzo Morra, Prof.

Abstract: Provence (SE France) was affected by two main phases of sporadic igneous activity during the Cenozoic. New 40Ar/39Ar laser step-heating data backdate the beginning of the oldest phase to late Eocene (40.82 ± 0.73 Ma ago), with activity present until early Miocene (~20 Ma ago). The products are mainly andesites, microdiorites, dacites and basaltic andesites mostly emplaced in the Agay-Estérel area. Major- and trace-element constraints, together with Sr-Nd-Pb isotopic ratios suggest derivation from a subcontinental lithosphere mantle source variably modified by subduction-related metasomatic processes. The overall composition of these rocks matches that of the products of the nearly coeval (emplaced ~38-15 Ma ago) late Eocene-middle Miocene magmatism of Sardinia. The genesis of dacitic rocks cannot be accounted by simple fractional crystallization alone, but possibly requires interaction of evolved melts with lower crustal lithologies or interaction of near-primitive melts with harzburgitic upper mantle rocks.
The youngest phase of igneous activity comprises basaltic volcanic rocks with mildly sodic alkaline affinity emplaced in the Toulon area ~10 Ma after the end of the previous subduction-related phase. These rocks show geochemical and isotopic characteristics akin to magmas emplaced in intraplate tectonic setting, indicating a sub-lithospheric HiMu+EM-II mantle source melting approximately in the spinel/garnet-lherzolite transition zone as the source region for such magmas. New 40Ar/39Ar laser step-heating data slightly pre-date the beginning of the volcanic activity to late Miocene-Pliocene (5.57 ± 0.09 Ma ago).
The emplacement of "anorogenic" igneous rocks a few Ma after that of "orogenic" rocks is a common feature in the Cenozoic districts of the Central-Western Mediterranean area. The origin of such "anorogenic" rocks can be explained with the activation of different mantle sources not directly modified by subduction-related metasomatic processes, possibly located in the sub-lithospheric mantle, and thus unrelated to the shallower lithospheric mantle source of the "orogenic" magmatism.

Cover letter

DIPARTIMENTO
DI SCIENZE DELLA TERRA

SAPIENZA
UNIVERSITÀ DI ROMA

Rome, April 27th 2017

Dear Editor,
Attached you find a manuscript submitted for publication in Lithos. This manuscript describes the geochemistry, mineralogy and petrography of Late Eocene-Miocene igneous rocks from SE France. This study is part of a larger study that is involving similar lithologies in Spain (Calatrava), Northern Africa (Algeria), Southern Italy and Sardinia.

A complete petrographic, mineral chemical and whole rock geochemical, including Sr-Nd-Pb isotopic survey has been carried out on these rocks. In addition, a detailed $^{40}Ar/^{39}Ar$ geochronological study allowed us to better constrain the origin of these rocks in a geodynamic framework.

We believe that the arguments treated in our manuscript are of great interest for the typical readership of Lithos, and for this reason we would like to submit it for publication.

On behalf of the co-authors,

Yours sincerely

Michele Lustrino

Università degli Studi di Roma La Sapienza
Dipartimento di Scienze della Terra
Piazzale Aldo Moro n. 5, 00185 Roma
Tel. (+39) 06 49914158 ax (+39) 06 4454729
michele.lustrino@uniroma1.it

Abstract

Provence (SE France) was affected by two main phases of sporadic igneous activity during the Cenozoic. New $^{40}Ar/^{39}Ar$ laser step-heating data backdate the beginning of the oldest phase to late Eocene (40.82 ± 0.73 Ma ago), with activity present until early Miocene (~20 Ma ago). The products are mainly andesites, microdiorites, dacites and basaltic andesites mostly emplaced in the Agay-Estérel area. Major- and trace-element constraints, together with Sr-Nd-Pb isotopic ratios suggest derivation from a subcontinental lithosphere mantle source variably modified by subduction-related metasomatic processes. The overall composition of these rocks matches that of the products of the nearly coeval (emplaced ~38-15 Ma ago) late Eocene-middle Miocene magmatism of Sardinia. The genesis of dacitic rocks cannot be accounted by simple fractional crystallization alone, but possibly requires interaction of evolved melts with lower crustal lithologies or interaction of near-primitive melts with harzburgitic upper mantle rocks.

The youngest phase of igneous activity comprises basaltic volcanic rocks with mildly sodic alkaline affinity emplaced in the Toulon area ~10 Ma after the end of the previous subduction-related phase. These rocks show geochemical and isotopic characteristics akin to magmas emplaced in intraplate tectonic setting, indicating a sub-lithospheric HiMu+EM-II mantle source melting approximately in the spinel/garnet-lherzolite transition zone as the source region for such magmas. New $^{40}Ar/^{39}Ar$ laser step-heating data slightly pre-date the beginning of the volcanic activity to late Miocene-Pliocene (5.57 ± 0.09 Ma ago).

The emplacement of “anorogenic” igneous rocks a few Ma after that of “orogenic” rocks is a common feature in the Cenozoic districts of the Central-Western Mediterranean area. The origin of such “anorogenic” rocks can be explained with the activation of different mantle sources not directly modified by subduction-related metasomatic processes, possibly located in the sub-lithospheric mantle, and thus unrelated to the shallower lithospheric mantle source of the “orogenic” magmatism.

- Two main igneous phases are recorded in SE France.
- New $^{40}Ar/^{39}Ar$ data backdate the beginning of the oldest phase to late Eocene.
- This is the first complete Sr-Nd-Pb isotopic study of these rocks.
- Ancient subduction has changed the sources of the subduction-related rocks.
- Anorogenic igneous rocks are emplaced a few Myr after that of "orogenic" phase.

Eocene-Miocene igneous activity in Provence (SE France): $^{40}Ar/^{39}Ar$ data, geochemical-petrological constraints and geodynamic implications

Michele Lustrino[1,2]*, Lorenzo Fedele[3], Samuele Agostini[4], Gianfranco Di Vincenzo[4], Vincenzo Morra[3]

1 = Dipartimento di Scienze della Terra, Sapienza Università di Roma - P.le A. Moro 5, 00185, Roma (Italy)

2 = CNR - Istituto di Geologia Ambientale e Geoingegneria (IGAG), c/o Dipartimento di Scienze della Terra, Sapienza Università di Roma - P.le A. Moro 5, 00185, Roma (Italy)

3 = Dipartimento di Scienze della Terra, dell'Ambiente e delle Risorse (DiSTAR), Università degli Studi di Napoli Federico II - Via Cupa Nuova Cinthia 21, 80126 Napoli (Italy)

4 = CNR - Istituto di Geoscienze e Georisorse (IGG), Via Giuseppe Moruzzi 1, 56124, Pisa (Italy)

* = corresponding author: michele.lustrino@uniroma1.it

Keywords: Provence, petrology, Mediterranean, geodynamics, subduction, $^{40}Ar/^{39}Ar$ geochronology, Sr-Nd-Pb systematic

Abstract

Provence (SE France) was affected by two main phases of sporadic igneous activity during the Cenozoic. New $^{40}Ar/^{39}Ar$ laser step-heating data backdate the beginning of the oldest phase to late Eocene (40.82 ± 0.73 Ma ago), with activity present until early Miocene (~20 Ma ago). The products are mainly andesites, microdiorites, dacites and basaltic andesites mostly emplaced in the Agay-Estérel area. Major- and trace-element constraints, together with

Sr-Nd-Pb isotopic ratios suggest derivation from a subcontinental lithosphere mantle source variably modified by subduction-related metasomatic processes. The overall composition of these rocks matches that of the products of the nearly coeval (emplaced ~38-15 Ma ago) late Eocene-middle Miocene magmatism of Sardinia. The genesis of dacitic rocks cannot be accounted by simple fractional crystallization alone, but possibly requires interaction of evolved melts with lower crustal lithologies or interaction of near-primitive melts with harzburgitic upper mantle rocks.

The youngest phase of igneous activity comprises basaltic volcanic rocks with mildly sodic alkaline affinity emplaced in the Toulon area ~10 Ma after the end of the previous subduction-related phase. These rocks show geochemical and isotopic characteristics akin to magmas emplaced in intraplate tectonic setting, indicating a sub-lithospheric HiMu+EM-II mantle source melting approximately in the spinel/garnet-lherzolite transition zone as the source region for such magmas. New $^{40}Ar/^{39}Ar$ laser step-heating data slightly pre-date the beginning of the volcanic activity to late Miocene-Pliocene (5.57 ± 0.09 Ma ago).

The emplacement of "anorogenic" igneous rocks a few Ma after that of "orogenic" rocks is a common feature in the Cenozoic districts of the Central-Western Mediterranean area. The origin of such "anorogenic" rocks can be explained with the activation of different mantle sources not directly modified by subduction-related metasomatic processes, possibly located in the sub-lithospheric mantle, and thus unrelated to the shallower lithospheric mantle source of the "orogenic" magmatism.

1. Introduction

During the Cenozoic, the Central-Western Mediterranean area was affected by a diffuse magmatism as a response to a complex geodynamic evolution (e.g., Lustrino and Wilson, 2007; Lustrino et al., 2011; Carminati et al., 2012; Faccenna et al., 2014). Many different

tectonic processes occurred during the last 40-50 Ma, leading to the development of two subduction systems with different polarity, consumption of both oceanic and continental lithosphere, attainment of continent-continent collision, slab break-off, slab roll-back and back-arc basin opening (Lustrino et al., 2009). The magmatic activity associated to these processes show both "subduction-related" (also defined as "orogenic") and "intraplate-like" (also defined as "anorogenic") geochemical characteristics (e.g., Lustrino and Wilson, 2007; Lustrino et al., 2011).

In Provence (SE France; Fig. 1) two different igneous phases developed during the Cenozoic. The oldest was mainly characterised by the emplacement of weakly to moderately porphyritic volcanic rocks with calcalkaline affinity, classically considered related with the originally NE-SW-trending, NW-directed Apennine-Maghrebide subduction system and date back to ~33 Ma ago. The youngest products, mainly consisting of weakly porphyritic to aphyric alkali basalts, were emplaced ~6 Ma ago, and appear to be geochemically unrelated with subduction-related source modifications. Understanding of this magmatism in the framework of Mediterranean geodynamics and correlation with coeval igneous rocks from nearby areas has been hindered by scanty geochemical and geochronological data.

In this study new petrographic, mineral chemical, whole-rock major- and trace-element, Sr-Nd-Pb isotopic data and $^{40}Ar/^{39}Ar$ ages for the Cenozoic volcanic rocks from Provence are presented (full details on the employed analytical techniques are in the ESM1). The new $^{40}Ar/^{39}Ar$ data allow us to extend back to the middle Eocene (~41 Ma ago, Lutetian/Bartonian boundary) the beginning of the subduction-related igneous activity in Provence. The presented geochemical data are compared with those for other coeval volcanic rocks from the Central-Western Mediterranean neighbouring areas (i.e., Sardinia, Alps, Corsica, Northern Apennines, Languedoc and Spain), with both "orogenic" and "anorogenic" geochemical signature, in order to unravel possible genetic relationships.

2. Geological framework

The geological history of the Central-Western Mediterranean area and surrounding regions is very complex and not yet fully agreed (e.g., Stampfli and Borel, 2002; Torsvik and Cocks, 2004; Rosenbaum et al., 2002; Lustrino et al., 2009; Turco et al., 2012; Weil et al., 2013; Faccenna et al., 2014; Casciello et al., 2015; Argnani et al., 2016). Starting from Paleozoic, the future Mediterranean area experienced numerous processes including 1) formation and consumption of several oceanic basins, 2) continental collisions, 3) back-arc basin extension, 4) subductions with different polarities and 5) diffuse igneous activity of extremely varied geochemical affinity. Although even the oldest of these events have certainly played some role in determining the composition of the mantle sources of the Cenozoic igneous rocks, in the following lines a focus on the Cenozoic to Present time span only is synthetically summarized.

The geodynamic evolution of the Central-Western Mediterranean from the end of the Mesozoic onwards is connected with the relative movements of three main plates (Europe, Africa and Adria), oceanic and transitional basins, plus an unknown number of smaller continental terranes (e.g., Carminati et al., 2012; Rosenbaum, 2014; Faccenna et al., 2014). Several authors proposed the existence of a continental terrane located in between the Alpine Tethys, dividing this ocean into a western branch (reported in literature as Nevado-Filabride, Maghrebian, Betic-Penninic, Western Ligurian or Piemontese-Liguride Ocean) and an eastern branch (reported in literature as Lucanian, Ionian, Eastern Ligurian, Mesogea Ocean or Eastern Tethys Branch or Sicilide Domain). This terrane played a key-role in determining the locus of the Alpine subduction system (e.g., Lustrino et al., 2009; Handy et al., 2010; Molli and Malavieille, 2011; Carminati et al., 2012). Doglioni (1991) and Doglioni et al. (1998) defined this terrane as the Mesomediterranean Terrane, while others (e.g., Boullin et al., 1986;

Dercourt et al., 1986; Guerrera et al., 1993; Michard et al., 2002; Molli, 2008; Belayouni et al., 2010) collectively called it as the AlKaPeCa block (acronym for Alboran-Kabilies-Peloritani-Calabria). Handy et al. (2010) proposed the existence of a short-lived early Mesozoic micro-plate that comprised both AlKaPeCa and adjacent western Ligurian Ocean, and called it Alkapecia.

The Alpine Orogeny led to the development of the Alpine-Betic and Dinaride Belts, preceded by the subduction of several Neotethyan and Alpine Tethyan oceanic branches (e.g., Carminati et al., 2010; Rosenbaum and Lister, 2005; Schmid et al., 2008; Handy et al., 2010). According to Handy et al. (2010), during the late Cretaceous the E-directed subduction of the western branch of the Alpine Tethys Ocean continued until the western margin of AlKaPeCa block collided with the southern European paleo-margin during early Eocene (Molli, 2008; Handy et al., 2010; Carminati et al., 2012). No igneous activity related to syn-subduction of oceanic lithosphere is recorded along the entire Alpine-Betic belt (Carminati et al., 2010). Due to its continental nature, the AlKaPeCa block did not enter the subduction zone, forcing the subduction to jump to the eastern branch of the Alpine Tethys. This caused the flip of the polarity subduction, giving birth to the Apennine-Maghrebide subduction system (Lustrino et al., 2009; Carminati et al., 2010, 2012, and references therein).

The new W-directed subduction led to a fast E-SE-directed roll-back of the subduction hinge, which caused the stretching of the upper plate lithosphere and the opening of a series of back-arc basins (Doglioni et al., 1999; Carminati et al., 2012), with a discontinuous thinning process that increases toward E-SE from the present-day coast of Provence. This caused important lateral thickness variations of the upper plate (e.g., Blundell et al., 1992; Panza et al., 2007), with the Sardinia-Corsica continental block, which also experienced a ~60° counter-clockwise rotation with a hinge approximately located in the Gulf of Genoa

(Gattacceca et al., 2007), representing the largest lithospheric ribbon in the Central-Western Mediterranean area (Carminati et al., 2012).

The continued continental lithosphere thinning to the E-SE eventually led to the formation of new oceanic crust in the Vavilov and Marsili Tyrrhenian basins (Kastens et al., 1988; Sartori, 1990). Some oceanic crust is also hypothesized to be present in the Ligurian-Provençal Basin (separating the Sardinia-Corsica block from the coast of Provence), but the presence of a thick sediment pile (up to 8 km) does not allow a direct sampling (e.g., Rollet et al., 2002). The opening of back-arc basins finally lead also to the total dismembering of the AlKaPeCa block, with the radial drifting of the terranes that composed it.

2.1. The Provence region

Provence is a region of south-eastern France characterised by a complex geological evolution (Bestani et al., 2015). Five major events influenced the present geological setting of Provence and the surrounding Gulf of Lion and Gulf of Genoa: 1) late Paleozoic Variscan continent-continent collision (e.g., Weil et al., 2013); 2) late Cretaceous-late Eocene compressional and transpressive tectonics related with the Pyrenean Orogeny (e.g., Lacombe and Jolivet, 2005; Jourdon et al., 2014); 3) late Eocene-Oligocene extension related with the development of the Central European Rift System (e.g., Ziegler and Dezes, 2007); 4) Miocene to Present N-S Alpine compression (e.g., Lacombe et al., 1992; Champion et al., 2000); 5) Oligocene-Miocene NE-SW-directed rifting to drifting associated with the opening of the Ligurian-Provençal Basin (e.g., Gattacceca et al., 2007).

The easternmost Provence basement is made up of plutonic and metamorphic rocks belonging to the southern Variscan Belt, once in crustal continuity with the same lithologies of the Sardinia-Corsica block (e.g., Elter et al., 2004). The crystalline basement consists mainly of phyllites, orthogneisses, meta-gabbros, meta-serpentinites, meta-peridotites and

migmatites, intruded by Carboniferous granites (e.g., Morillon et al., 2000; Elter and Pandeli, 2005 and references therein).

Provence can be subdivided into a western and eastern domain (Fig. 1) by the main Mid-Durance Fault System (MDF), which is connected southwards to the Aix-en-Provence fault (AF; Cushing et al., 2008; Terrier et al., 2008). Western Provence features a thick (up to 10 km) Meso-Cenozoic sedimentary succession deposited in shelf basins, while eastern Provence is characterised by much thinner (2-3 km) coeval sedimentary pile and includes crystalline and metamorphic Variscan basement and Paleozoic rocks.

During the late Cretaceous and Eocene, tectonic evolution was dominated by N-S compression (e.g., Bestani et al., 2015), which also led to the development of the Pyrenean belt during the Eocene. After that, an extensional phase developed in central Europe, involving most of the Variscan basement along the Alpine and Pyrenean foreland (e.g., Ziegler and Dézes, 2007), leading to the formation of several rift-related basins (i.e., Rhine and Rhone Grabens). Such event was recorded also in SE France, with E-SE extension that partially truncated the Pyrenean-Provence thrust belt. During the Oligocene, a second extensional phase, related with the opening of the Ligurian-Provençal basin, led to the first SE-directed rifting of the Sardinia-Corsica block, then followed by drifting and counter-clockwise rotation with respect to the southern Europe paleo-margin (e.g., Gueguen et al., 1998; Sérrane, 1999; Gattacceca et al., 2007). The latter extensional phase led to the new transtensional reactivation of the NE-trending Nimes and Aix-Durance Faults (Séranne et al., 1995). The N-S Miocene to Present Alpine compression affecting mainly the western Provence (Lacombe et al., 1992; Champion et al., 2000) was responsible for the activation of S-verging thrusts West to the Aix-Durance Fault. On the other hand, the eastern Provence was not affected by the Alpine compression and the Pyrenean deformation is thus well preserved (Combes, 1984).

175

176 **2.2. Cenozoic magmatism of Provence**

177 The first late Paleogene phases of igneous activity recorded in the embryonic Western
178 Mediterranean are generally set in an "orogenic" framework, characterised by the NW-
179 directed Apennine-Maghrebian subduction beneath the European southern paleo-margin in
180 the Africa-Europe convergence contest (e.g., Lustrino et al., 2009, 2011). The age of the onset
181 of subduction is not yet clearly defined, with hypotheses ranging from the late Cretaceous
182 (e.g., Faccenna et al., 1997), to late Eocene (Lustrino et al., 2009) or early Oligocene
183 (Gueguen et al., 1998).

184 Available stratigraphic and radiometric constraints suggest that the igneous activity of
185 Provence developed in two distinct phases. The first one was mainly characterised by the
186 emplacement of calcalkaline pyroclastic to effusive rocks (plus much rarer sub-volcanic
187 bodies), with a geochemical signature resembling that of subduction-related igneous rocks
188 (e.g., Beccaluva et al., 1994). The oldest dated products (~33-31 Ma) are Le Dramont
189 microdiorites (locally called "*estérellites*"), together with andesitic and dacitic clasts within
190 the Saint-Antonin pyroclastic deposits (Féraud et al., 1996). These were followed by basaltic,
191 andesitic and dacitic lavas and pyroclasts, cropping out around Villeneuve-Loubet, and by
192 andesites dated 26.2 ± 1.0 Ma (Bellon and Brousse, 1971), cropping out between Biot and
193 Grasse. More recently, during the construction of the railway tunnel between Monaco and
194 Cap-d'Ail, two pyroclastic levels were dated by the K/Ar method, yielding ages of ~27 and
195 ~19 Ma (Ivaldi et al., 2003), the latter representing the latest manifestation of such
196 magmatism. The new $^{40}Ar/^{39}Ar$ ages reported here shift back to late Eocene the beginning of
197 this magmatic cycle (see section 3.3), which will be therefore referred to as the "Late Eocene
198 to Early Miocene" (LEEM) magmatism.

199 The second phase occurred during late Miocene to Pliocene (hereafter LMP), after a time
200 gap of ~10 Ma. The products consist of mildly sodic alkali basalts resembling magmas
201 emplaced in intraplate settings. The few available geochronological data refer mainly to rocks
202 from the Toulon area, which yielded $^{40}Ar/^{39}Ar$ ages of 6.97 ± 0.24 and 6.30 ± 0.22 Ma
203 (unpublished data quoted in Rehault et al., 2012), and one K/Ar age, without uncertainty, of 6
204 Ma (Baubron, 1974).
205
206 **2.3. Distribution of magmatism in neighbouring areas**
207 The Cenozoic magmatism of Provence shares many similarities with the basically coeval
208 magmatism of some of the neighbouring areas. This is particularly true for Sardinia and
209 offshore Corsica, because, before the Oligocene rifting and the Miocene drifting, the Sardinia-
210 Corsica block was part of the southern European paleo-margin, and thus in crustal continuity
211 with Provence. In the following lines a brief summary of the main characteristics of such
212 coeval igneous cycles is presented.
213 Sardinia was affected by two distinct Cenozoic magmatic episodes, similar to those of
214 Provence. The first phase lasted from ~38 to ~15 Ma ago (e.g., Morra et al., 1994, 1997;
215 Lecca et al., 1997; Lustrino et al., 2004, 2009, 2013; Conte et al., 2010; Guarino et al., 2011),
216 with a peak at around ~22-18 Ma ago, and emplaced mostly arc-tholeiitic and calcalkaline
217 rocks interpreted as related with the NW-directed Apennine subduction system. Dacitic to
218 rhyolitic ignimbrites prevail, followed by andesites, basaltic andesites and minor High-Mg
219 and High-Al basalts. The late subduction-related activity was characterised by high-K
220 calcalkaline terms in the middle Miocene (e.g., Beccaluva et al., 2013). The second igneous
221 episode occurred after a few Ma of quiescence, from early late Miocene (~12 Ma ago) to
222 Pleistocene (~0.1 Ma ago), and emplaced mainly sodic to tholeiitic basalts that seem
223 geochemically unrelated to active or ancient subduction systems (e.g., Beccaluva et al., 1985;

224 Gasperini et al., 2000; Lustrino et al., 2000, 2004, 2007a,b, 2009, 2011, 2013). Lustrino et al
225 (2000) subdivided the middle Miocene-Pleistocene volcanic rocks into two types from a Pb-
226 Nd-Sr isotope point of view. The RPV group (Radiogenic Pb Volcanics) comprises the oldest
227 (~11.8-4.4 Ma) and rarest products cropping out in southern Sardinia only. On the other hand,
228 the UPV group (Unradiogenic Pb Volcanics) comprise the much more abundant rocks (>99%
229 of the total) emplaced from ~4.8 to 0.1 Ma ago in the central and northern sectors of the
230 island, showing unique isotopic signature in the framework of the CiMACI province (Circum-
231 Mediterranean Anorogenic Cenozoic Igneous; Lustrino and Wilson, 2007).
232 In NE Corsica the only evidences of Cenozoic magmatic activity are represented by the
233 Sisco lamproite dyke (~15 Ma; Peccerillo et al., 1988; Conticelli et al., 2002), whereas in
234 southern Corsica (Balistra, Tre Paduli and Francolu localities) limited rhyolitic ignimbrites
235 dated ~19 Ma (Ottaviani-Spella et al., 1996, 2001) crop out. Offshore Corsica two main
236 volcanic fields were distinguished (Réhault et al., 2012). The first is located to the SW, along
237 the northward prolongation of the central Sardinian Rift, characterised by the emplacement of
238 mainly basaltic andesites and andesitic magmas with calcalkaline and high-K calcalkaline
239 affinity between ~21 and 13 Ma ago. The second volcanic field is located NW of Corsica,
240 with products ranging in age between ~14 and 6 Ma, represented by alkali basalts dredged in
241 the Monte Doria volcanic complex. The strong alteration of many of such submarine rocks
242 (with LOI up to 22 wt.%) likely caused serious problems in $^{40}Ar/^{39}Ar$ dating. Interestingly,
243 Réhault et al. (2012) report the K/Ar age of 43.00 ± 2.34 Ma for a pillow andesite clast
244 dredged along the Tristanite Ridge in NW Corsica, possibly related to the ~38 Ma
245 microdiorite of Calabona (Alghero, NW Sardinia; Lustrino et al., 2009).
246 The main Cenozoic igneous rocks cropping out in the Alpine region are mostly associated
247 with the Periadriatic dextral trascurrent fault system. Radiometric ages range from ~42 to 24
248 Ma, with a peak around Rupelian (~34-28 Ma ago; von Blanckenburg and Davies, 1995;

Rosenberg, 2004). The products are mainly of calcalkaline and high-K calcalkaline affinity, with minor potassic and ultrapotassic terms (references in Lustrino et al., 2011).

In the southern Iberian Peninsula, a Cenozoic magmatic cycle with subduction-related geochemical characteristics developed along the Betic Cordillera (southern Spain, ~38-6 Ma; Turner et al., 1999; Duggen et al., 2004), with products mainly represented by andesites and dacites with subordinate rhyolites and shoshonites. A younger magmatic phase at ~2.9-2.3 Ma ago emplaced Na-rich basic rocks (mostly hawaiites) in the Cartagena-Tallante area with "anorogenic" signature (Duggen et al., 2005; Cebrià et al., 2009).

Finally, the Languedoc volcanic province was characterised by prolonged scattered alkali basaltic activity spanning from ~160 to 0.5 Ma ago. Such a low-volume (~2 km^3), long-lasting, geochemically homogenous activity within a very narrow area is somewhat puzzling and still not fully understood (Dautria et al., 2010). A progressive southward rejuvenation of the magmatic activity in Languedoc is clear for the last 7 Ma, whereas it is not recorded for the pre-Miocene activity.

3. Results

3.1. Petrography

The collected Cenozoic igneous rock samples from Provence belong mainly to the LEEM phase (30 samples), plus a smaller number (4 samples) from the LMP phase. Their main petrographic features are presented below (Fig. 2).

The LEEM rocks are mainly represented by intermediate "andesitic" rocks (24 samples) showing weakly to moderately porphyritic seriate texture (P.I. ~10-30%; P.I. = porphyritic index = % area occupied by phenocryst over total thin section) and a paragenesis consisting of plagioclase plus minor clinopyroxene and amphibole. Plagioclase typically accounts for ~90% of the total phenocrysts (up to 2 mm in length) and commonly exhibits a "cribrose" (sieved)

core and complex oscillatory zoning. Clinopyroxene is ~5-10% of the total phenocryst load and is represented by colourless to pale green small crystals with opaque oxide inclusions. Pale brown to green amphibole is only rarely observed as a phenocryst, mostly in rocks with lower clinopyroxene content, and is typically rimmed with opaque oxides. Groundmass ranges from hypocrystalline to hypohyaline and is made up essentially by plagioclase with minor clinopyroxene, diffuse opaque oxides and occasional orthopyroxene microcrysts.

A smaller aliquot of the collected LEEM rocks (6 samples) is represented by moderately porphyritic (P.I. ~25-40%) evolved "dacitic" rocks, with abundant plagioclase and subordinate quartz and amphibole. Plagioclase is the dominant phenocryst phase (>90% of the total, reaching up to 5 mm in length), followed by much rarer anhedral quartz and sporadic brown to yellow amphibole. Small clusters of chlorite and opaque oxides were also occasionally found, possibly representing former biotite microphenocrysts. Groundmass is typically hypohyaline and features plagioclase, quartz, diffuse opaque minerals and minor clinopyroxene.

The LMP rocks are represented by "basaltic" rocks displaying weakly porphyritic to aphyric (occasionally ophitic to sub-ophitic) textures, with a paragenesis mainly consisting of plagioclase, olivine and clinopyroxene. Though being by far the most abundant mineral phase (80-90% of the total), plagioclase is rarely found as a phenocryst, mainly occurring as small groundmass phase. Olivine is the main phenocryst, represented by crystals up to 1 mm in length and commonly displaying thin iddingsite rims. Groundmass is hypocrystalline and basically consists of plagioclase, clinopyroxene, olivine and opaque microcrysts.

3.2. Mineral chemistry

297 Selected representative samples from the LEEM (andesitic and dacitic) and LMP (basaltic)
298 rocks were analysed for the determination of the composition of the main mineral and glass
299 phases. The results are reported in Electronic Supplementary Material (ESM) 2.1 to 2.6.

300 Feldspars. Plagioclase is the most abundant phase in all the investigated rocks, where it
301 covers a wide compositional span from andesine to anorthite ($An_{32-91}Ab_{8-65}Or_{0-13}$; Fig. 3a).
302 Plagioclase from the LEEM "andesitic" rocks basically covers the entire above compositional
303 range, with only small differences between phenocryst core ($An_{48-90}Ab_{10-49}Or_{0-3}$), phenocryst
304 rim ($An_{34-91}Ab_{8-62}Or_{0-3}$) and groundmass microcrysts ($An_{32-80}Ab_{19-55}Or_{0-13}$). On the other
305 hand, plagioclase from LEEM "dacitic" rocks shows a remarkably more homogeneous
306 andesinic composition, for both phenocryst core ($An_{34-40}Ab_{59-65}Or_1$) and phenocryst rim
307 ($An_{35-46}Ab_{53-64}Or_1$). As regards LMP "basaltic" rocks, plagioclase displays a relatively limited
308 compositional range, from bytownitic phenocryst cores ($An_{75}Ab_{25}Or_0$) to labradoritic
309 phenocryst rims ($An_{69}Ab_{30}Or_1$), up to labradoritic-andesinic groundmass laths ($An_{48-67}Ab_{32-50}Or_{1-2}$).

311 The only alkali feldspar crystal analysed was found in a LEEM "andesitic" sample,
312 showing a Na-rich sanidine composition ($An_{10}Ab_{55}Or_{35}$).

313 Pyroxenes. Clinopyroxene is the main ferromagnesian phase of the "andesitic" and
314 "basaltic" rocks, where it mainly ranges from diopside to augite plus rarer pigeonite
315 compositions (Fig. 3b). In LEEM "andesitic" rocks, the few Ca-rich clinopyroxene crystals
316 range from diopside ($Wo_{45}En_{41}Fs_{14}$, with Al = 0.094 apfu, Mg# = 0.83), to aluminian diopside
317 ($Wo_{45}En_{42}Fs_{130.82}$, Al = 0.102 apfu, Mg# = 0.82; "aluminian" indicates Al >0.10 apfu;
318 Morimoto et al., 1988), up to aluminian-ferrian diopside ($Wo_{45-46}En_{40-41}Fs_{12-20}$, Al = 0.131-
319 0.154 apfu, Mg# = 0.88-0.93). Most of LEEM clinopyroxenes are of the augitic type (in a
320 continuous transition with the diopsidic ones), with compositions ranging from augite (Wo_{39-45}-$En_{39-44}Fs_{14-21}$, Al = 0.037-0.131 apfu, Mg# = 0.70-0.83), to aluminian-ferrian augite (Wo_{42-}

$_{44}En_{40-42}Fs_{14-17}$, Al = 0.102-0.152, Mg# = 0.81-0.89) and ferrian augite ($Wo_{39-43}En_{40-43}$-Fs_{15-19}, Al = 0.054-0.098 apfu, Mg# = 0.76-0.84). A few subcalcic pigeonite crystals have also been found as groundmass phase only (Wo_{7-11}-En_{54-62}-Fs_{31-35}), showing very variable Al (0.048-0.206 apfu) and lower Mg# (0.62-0.71) with respect to LEEM clinopyroxenes. No significant differences have been found between core, rim and groundmass clinopyroxenes of all the above three varieties.

Some orthopyroxene crystals were also found in the groundmass of LEEM "andesitic" rocks only. Crystals fall in the enstatite field, displaying a quite variable compositional range ($Wo_{3-4}En_{57-67}Fs_{30-40}$; Fig. 3b) with Mg# = 0.60-0.72.

Clinopyroxenes from LMP rocks are aluminian diopside ($Wo_{45}En_{38-40}Fs_{15-16}$, Al = 0.142-0.159 apfu, Mg# = 0.76-0.80) and aluminian-ferrian diopside ($Wo_{45}En_{36}Fs_{19}$, Al = 0.153-0.189 apfu, Mg# = 0.74-0.78), displaying a distinctively Ti-richer composition (0.048-0.093 apfu) with respect to LEEM clinopyroxenes (Ti = 0.007-0.028 apfu).

Olivine. Olivine was found in the LMP "basaltic" rocks only. It is characterized by a variable forsterite content (Fo_{60-82}), decreasing quite linearly from phenocryst cores (Fo_{77-82}) to phenocryst rims (Fo_{72-77}) and groundmass microcrysts (Fo_{60-75}).

Amphibole. Amphibole was rarely observed in LEEM "andesitic" rocks, displaying pargasitic (e.g., Ca = 1.775-1.904 apfu, Fe^{3+} = 0.200-0.303 apfu, Mg# = 0.65-0.74) and magnesio-hastingsitic compositions (Ca = 1.758-1.979 apfu, Fe^{3+} = 0.240-0.622 apfu, Mg# = 0.65-0.82), both occasionally Ti-rich (i.e., Ti >0.30 apfu). Phenocryst core and rim compositions are basically undistinguishable, although the first is generally Mg-richer (Mg# = 0.68-0.82 vs. 0.65-0.78).

Opaque oxides. In LEEM "andesitic" rocks, opaque oxides are represented by sparse groundmass crystals belonging to the magnetite-ulvöspinel series. The composition is quite

346 variable, with relatively low Al (0.002-0.196 apfu), Mg (0.019-0.152 apfu) and Cr (<0.008
347 apfu) and ulvöspinel content ranging from 6.70 to 52.1 mol.%.

348 In the LMP rocks, groundmass opaque oxides belong both to the spinel and the hematite-
349 ilmenite rhombohedral series. The LMP spinel crystals are generally poorer in Al (0.008-
350 0.015 apfu) and Cr (<0.003 apfu) and richer in Mg (0.126-0.324 apfu) and Ti (ulvöspinel
351 content ranging from 69.0 to 85.3 mol.%.) with respect to their LEEM counterparts. The LMP
352 rhombohedral opaques are have low Al (<0.005 apfu), Cr (<0.001 apfu), variable Mg (0.013-
353 0.149 apfu), and very high Ti (ilmenite content ranging from 87.2 to 100 mol.%).

354 Glass. The groundmass glass analysed from two LEEM "andesitic" samples displays a
355 relatively homogeneous rhyolitic composition (SiO_2 = 69.9-72.0 wt.%, Al_2O_3 = 11.3-12.3
356 wt.%, MgO = 0.16-0.26 wt.%, CaO = 0.68-0.88 wt.%, Na_2O+K_2O = 7.85-8.57 wt.%).

357

358 **3.3. $^{40}Ar/^{39}Ar$ data**

359 Two groundmass and three plagioclase concentrates were analysed by the $^{40}Ar/^{39}Ar$ laser
360 step-heating technique in order to refine geochronological data. Details on the analytical
361 procedures and the full analytical dataset are given in the ESM1 and in ESM2.7, respectively.
362 Age and K/Ca spectra are shown in Fig. 4 and results are summarized in Table 1.

363 The three plagioclase separates from the rocks of the LEEM group yielded internally
364 discordant age profiles with overall saddle shapes, which may be diagnostic of excess Ar
365 (parentless ^{40}Ar; e.g., Kelley, 2002). Total gas ages are in the range of ~33 Ma (FEM4) to ~47
366 Ma (FEM30) and step ages mainly within ~31-52 Ma.

367 Thirteen consecutive steps from the intermediate- to high-temperature region of
368 plagioclase from the "andesitic" sample FEM4 (Monaco location) gave a concordant segment
369 representing ~78% of the total $^{39}Ar_K$ released, yielding an error-weighted mean age of 32.64 ±
370 0.80 Ma. The concordant segment is characterised by lower K/Ca ratios (derived from

neutron-produced Ar isotopes) than those from lower temperature steps and decreasing values (from 0.15 to 0.02) with increasing temperature. A least-squares fit in an isochron diagram ($^{36}Ar/^{40}Ar$ vs. $^{39}Ar/^{40}Ar$ three-isotope correlation plot) for the same set of data yields a slight nominally younger intercept age of 32.47 ± 0.78 Ma and a not well-defined initial $^{40}Ar/^{36}Ar$ ratio of 305 ± 30, indistinguishable from that of modern atmospheric Ar ($^{40}Ar/^{36}Ar$ ~290-300). The preferred age of 32.64 ± 0.80 Ma is 6 to ~14 Ma older than previously published K/Ar whole-rock ages for two pyroclastic levels sampled from the same locality (18.7 ± 0.8 Ma and 27.0 ± 0.8 Ma; Ivaldi et al., 2003).

Plagioclase separates from the "andesitic" sample FEM23 (Villeneuve-Loubet) gave the most pronounced saddle-shaped age spectrum and a K/Ca profile comparable to that of sample FEM4. The minimum of the saddle is defined by seven concordant steps, representing ~50% of the total $^{39}Ar_K$ released and yielding an error-weighted mean age of 32.41 ± 0.48 Ma. A least-square fit in an isochron plot using data from the same heating steps yields a nominally younger intercept age of 31.77 ± 0.81 Ma and an initial $^{40}Ar/^{36}Ar$ ratio of 330 ± 32, significantly higher than that of modern atmospheric Ar. The inclusion of the subsequent two steps, solely based on their linearity, yields a slightly younger intercept age of 31.40 ± 0.84 Ma and an initial $^{40}Ar/^{36}Ar$ ratio (361 ± 27), again significantly higher than of modern atmospheric Ar. Bellon and Brousse (1971) reported a ~5 Ma younger K/Ar age for an andesite sample from a nearby location (Biot and Grasse).

Plagioclase separates from the "dacitic" sample FEM30 (Agay-Estérel) gave a concordant segment from the intermediate- to high-temperature region, representing ~67 % of the total $^{39}Ar_K$ released and yielding an error-weighted mean age of 40.87 ± 0.80 Ma. K/Ca ratios are nearly constant over the nine concordant steps (range of 0.039 ± 0.005 to 0.031 ± 0.004). A least-squares fit in an isochron plot using the same heating steps yields a not well-defined age of 39.3 ± 2.7 Ma and initial $^{40}Ar/^{36}Ar$ ratio of 339 ± 75, indistinguishable, within error, with

that of modern atmospheric Ar. Close to the sampling area, Fèraud et al. (1996) obtained a significantly younger $^{40}Ar/^{39}Ar$ plateau age of 32.7 ± 0.9 Ma for Le Dramont microdiorites (locally called "*estérellites*"). Interestingly, the age of ~41 Ma extends back the onset of Cenozoic igneous activity in Provence to the Lutetian/Bartonian boundary, thus comparing remarkably well with the oldest volcanic manifestation known in Sardinia (Alghero Calabona microdiorite, 38.28 ± 0.26 Ma; Lustrino et al., 2009).

As for the LMP rock samples, groundmass from the basalt FEM33 (Hyéres) yielded a nearly flat age spectrum, characterized by a concordant segment for ~99% of the total $^{39}Ar_K$ released, with an error-weighted mean ages of 5.57±0.09 Ma. Groundmass of basalt FEM35 (Toulon) gave a slightly more disturbed age profile. However, four consecutive steps, with a constant K/Ca ratios and representing ~58% of the total $^{39}Ar_K$ released, gave an error-weighted mean age of 5.67 ± 0.16 Ma, which is indistinguishable at 1σ level from the mean age of groundmass FEM33. The two new ages are slightly but significantly younger (0.73 ± 0.24 Myr) than literature data for products of the youngest Cenozoic igneous cycle of Provence (unpublished data quoted in Réhault et al., 2012).

3.4. Whole-rock geochemistry

The intermediate "andesitic" rocks of the LEEM group fall in the fields of basaltic andesite (plus one trachybasaltic andesite) and andesite (SiO_2 = 54.1-62.7 wt.%, Na_2O+K_2O = 4.17-5.94 wt.%), whereas the few evolved "dacitic" rocks can be classified as dacite (SiO_2 = 63.1-65.9 wt.%, Na_2O+K_2O = 4.74-6.19 wt.%), with the only exception of one sample straddling the andesite/dacite fields (Fig. 5). They fall well within the field for subalkaline rock series, representing a medium-K/high-K series or a medium-Fe/high-Fe tholeiitic series (though some of the SiO_2-richest samples fall in the low-Fe calcalkaline realm; Fig. 6). The "basaltic" LMP rocks display a much narrower compositional spectrum, falling in the basalt field (SiO_2

421 = 48.4-51.4 wt.%, Na_2O+K_2O = 3.93-4.72 wt.%) and straddling the divide between
422 subalkaline and alkaline basalts (Fig. 5). Given their notably higher Na_2O with respect to K_2O
423 (3.47-3.84 vs. 0.46-1.17 wt.%; Table 2, ESM2.8), LMP rocks are considered to belong to an
424 alkaline sodic series (i.e., $Na_2O \geq K_2O + 2$).

425 When binary variation diagrams vs. SiO_2 are taken into account (Figs. 7 and 8 and ESM3
426 and 4) intermediate and evolved LEEM rocks seem to depict an overall coherent evolutionary
427 trend for many major and trace elements (e.g., see decreasing TiO_2, Fe_2O_3, Al_2O_3, CaO, P_2O_5,
428 V and Y, increasing Na_2O, Ba and Nb and K_2O, and Rb firstly increasing then decreasing).
429 Some major scattering can be however envisaged, especially in the "andesitic" rocks, for the
430 trends of Al_2O_3, MgO (0.85-3.72 wt.% in the basaltic andesites and andesites, 2.20-3.61 wt.%
431 in the dacites), Na_2O, Sr (301-423 and 323-415 ppm), Rb, Ba, Y and Zr (76-276 and 65-111
432 ppm). Other occasional deviations (e.g., see the andesite with anomalously high 11.8 wt.%
433 CaO or the two with relatively high Nb, similar to that of dacites) may be ascribed to post-
434 emplacement modifications (e.g., secondary calcite for the first; see the high LOI ≥5 wt.%).

435 When compared with neighbouring coeval "subduction-related" products (from Sardinia,
436 Alps, N-Apennine, Corsica-Estérel and Spain) of comparable SiO_2 ranges, LEEM rocks show
437 many similarities, for both absolute concentrations and evolutionary trends. The main
438 differences are those regarding: 1) generally higher Na_2O for LEEM rocks; 2) Large Ion
439 Lithophile Elements (LILE; Cs, Rb, Sr, Ba) showing much wider spectra in the neighbouring
440 districts (especially the Alps, likely due to the extremely variable rock composition, from arc-
441 tholeiites to calcalkaline, high-K calcalkaline up to lamproitic/lamprophyric; Lustrino et al.,
442 2011); 3) remarkably lower Y, Pb, Th and U for LEEM rocks.

443 The LMP basaltic rocks display relatively narrow compositional spectra, with higher TiO_2
444 (1.47-2.43 wt.%), Fe_2O_3 (11.3-11.9 wt.%), MgO (5.76-8.48 wt.%), Cr (110-240 ppm) and Ni
445 (110-160 ppm), and lower Al_2O_3 (15.1-16.6 wt.%) with respect to LEEM rocks. The four

446 investigated samples typically define two distinctive compositional clusters, with sample
447 FEM31 systematically plotting away from the other three samples due to its much lower SiO_2,
448 TiO_2, K_2O, P_2O_5, Sr, Ba, Cr, Ni and Nb, and higher Al_2O_3, MgO, CaO, V and Y.
449 With respect to neighbouring coeval "anorogenic" products (Sardinia RPV and UPV,
450 Languedoc and Spain igneous rocks) of similar degree of differentiation, LMP rocks display
451 an overall similar composition for most major- and trace elements. Some main differences can
452 be noticed for the generally higher CaO and Y and lower K_2O, P_2O_5, Rb, Sr, Ba, Cr, Ni, Zr
453 and Nb for LMP rocks. These are particularly evident for sample FEM31 that, due also to its
454 much lower TiO_2 commonly falls in the field depicted by the "subduction-related" Cenozoic
455 igneous rocks.
456
457 **3.5. Primitive mantle-normalized diagrams**
458 Multi-element primitive-mantle normalized diagrams for the LEEM and LMP rocks are
459 reported in Fig. 9. The LEEM rocks show highly spiked patterns, with marked troughs at Nb-
460 Ta-Ti and peaks at Cs-K-Pb peaks, resulting in the high LILE/HFSE ratios (HFSE = High
461 Field Strength Elements) typical for subduction-related magmas. The concentration of the
462 other HFSE Zr and Hf is particularly high, resulting in a clear hump in normalized patterns.
463 The overall pattern of the LEEM rocks resemble closely that of GLOSS-II (Global subducting
464 sediment estimate; Plank, 2014), although the latter shows slightly higher enrichment in fluid-
465 mobile elements, such as LILE and Th-U, and slightly higher concentrations for the Rare
466 Earth Elements (REE).
467 The general pattern for basaltic andesite and andesite is largely similar, showing roughly
468 the same HFSE contents and nearly flat medium and heavy REE (MREE and HREE),
469 clustering around 5-8 times primitive mantle (PM) abundances. The dacitic rocks display
470 similar sub-parallel trends, with higher abundances of strongly incompatible elements (e.g.,

higher peak at Cs), more evident Ti trough, smaller Nb-Ta troughs, and generally lower abundances for the progressively less incompatible elements (e.g., LREE, Zr and Hf), coupled with and M-HREE clustering around 2-4 PM estimate).

The main differences with the products from coeval neighbouring Central-Western "subduction related" districts (not shown) include: 1) higher peaks at fluid-mobile elements (e.g., Th-U) for the rocks from the Alps, Sardinia and Spain; 2) Rb-Ba troughs and deeper Nb-Ta troughs for the rocks from Sardinia and Spain; 3) a Rb trough for the rocks from N-Apennines; 4) higher Pb peaks for the rocks from N-Apennines and Spain.

As regards LMP rocks, FEM31 clearly emerges as an outlier sample compared to the rest of the rocks (FEM33, 34 and 35). All the LMP rocks but FEM31 have smoother patterns, with normalized abundances rarely exceeding ~80 PM, limited peaks at Nb-Ta and low and fractionated HREE contents (clustering around 5-7 PM). Such patterns share numerous similarities with those for St. Helena basalts, the classical HiMu-OIB type-locality (i.e., Ocean Island Basalt with the *high-μ* geochemical signature of a mantle source with a component of ancient and recycled oceanic crust; e.g., Kawabata et al., 2011; Stracke, 2012). Sample FEM31 is characterised by: 1) Nb-Ta troughs, definitely uncommon for intraplate-setting rocks; 2) low Nb/Nb* [0.5, compared to the other LMP rocks with 1.4-1.6; Nb/Nb* = $Nb_N/(K_N*U_N)^{1/2}$, N = primitive mantle-normalized]; 3) Ba trough; 4) marked Cs peak (~2500 PM); 5) lower LREE and MREE; 6) flat HREE pattern (~8-10 PM).

When compared with the coeval neighbouring "anorogenic" products (not shown), LMP rocks (excluding FEM31) show remarkably similar patterns, especially with respect to the igneous rocks from Languedoc. The RPV rocks from Sardinia have slightly higher incompatible element contents (e.g., LILE) and a small Ti trough, whereas UPV rocks from Sardinia have a deep Rb trough, a marked Ba peak and lower HREE contents. "Anorogenic"

495 rocks from Spain display generally higher incompatible element abundances (especially for
496 LILE) and a marked K trough.
497
498 **3.6. Isotope systematic**
499 The results of Sr-Nd-Pb isotope analyses are reported in Table 2. Measured values were
500 recalculated on the basis of the new $^{40}Ar/^{39}Ar$ ages: 32 Ma for LEEM basaltic andesites and
501 andesites, 41 Ma for LEEM dacites and 6 Ma for LMP alkali basalts.
502 LEEM group rocks cover a limited span of initial $^{87}Sr/^{86}Sr$, from 0.70526 to 0.70604 in
503 andesites to 0.70449 in dacites. On the other hand, initial $^{143}Nd/^{144}Nd$ shows a larger
504 variability, with andesites ranging from 0.512489 to 0.512615, while the only dacite analyzed
505 has more radiogenic $^{143}Nd/^{144}Nd$ (0.512912). No clear correlation with SiO_2 is observed for
506 both isotopic ratios (see ESM5). Compared with the coeval "subduction-related" rocks from
507 neighbouring areas, LEEM samples fall on the least Sr-radiogenic and most Nd-radiogenic
508 end (Fig. 10a).
509 The LMP rocks are characterised by quite constant relatively low $^{87}Sr/^{86}Sr$ (0.70358-
510 0.70430) and relatively high $^{143}Nd/^{144}Nd$ (0.512734-0.512828), falling in the same isotopic
511 field identified by the coeval anorogenic rocks of Sardinia RPV group and of Languedoc.
512 Both LEEM and LMP rocks plot along a hypothetical tie-line connecting DMM (Depleted
513 MORB Mantle) and EM-II (Enriched Mantle II) mantle components.
514 As for Pb isotopes, LEEM rocks show a quite homogeneous composition, with $^{206}Pb/^{204}Pb$
515 = 18.6-18.7, $^{207}Pb/^{204}Pb$ = 15.6-15.7, $^{208}Pb/^{204}Pb$ = 38.6-38.7, with the dacite plotting within
516 the field of the andesitic rocks (Figs. 10b,c,d). Again, no correlation is observed with SiO_2
517 contents (see ESM6) The investigated samples fall well within the field defined by coeval
518 neighbouring districts of similar geotectonic setting, typically plotting above the Northern

519 Hemisphere Reference Line (NHRL), between the DMM, HiMu-OIB and EM-II components,
520 and to the right of the 4.56 Ga Geochron.

521 The LMP rocks show relatively homogeneous Pb isotopic ratios, with slightly more
522 uranogenic ($^{206}Pb/^{204}Pb$ = ~18.9, $^{207}Pb/^{204}Pb$ ~15.7) and more thorogenic ($^{208}Pb/^{204}Pb$ = 38.9-
523 39.1) Pb compositions with respect to LEEM rocks. They also fall above the NHRL between
524 the DMM, HiMu-OIB and EM-II components and to the right of the 4.56 Ga Geochron.
525 Interestingly, rocks from Languedoc and Spain straddle the NHRL and plot mostly below it,
526 while UPV Sardinia rocks display markedly unradiogenic $^{206}Pb/^{204}Pb$ (~17.4-18.1) and
527 $^{208}Pb/^{204}Pb$ (~37.4-38.2) that plot them to the left of the 4.56 Ga Geochron and suggest the
528 involvement of a EM-I (Enriched Mantle I) mantle component (Lustrino and Dallai, 2003).

529 No clear correlation seems to exist between Pb and Sr isotope ratios for both LEEM and
530 LMP rocks (Fig. 11). The "subduction-related" rocks from the Central-Western
531 Mediterranean have generally constant Pb isotopic composition (except for some $^{207}Pb/^{204}Pb$
532 variability), coupled with much more variable $^{87}Sr/^{86}Sr$ (~0.703-0.719). On the other hand,
533 "anorogenic" rocks display an overall constant $^{87}Sr/^{86}Sr$ coupled with a large variation of Pb
534 isotope ratios (and a marked gap separating Pb-radiogenic LMP, Languedoc, Spain and
535 Sardinia RPV products from Pb-unradiogenic Sardinia UPV rocks).

536

537 # 4. Discussion

538 ## 4.1. Disequilibrium in the LEEM rocks

539 The LEEM rocks display the typical petrographic, mineralogical and geochemical features
540 of subduction-related products such as: 1) porphyritic textures dominated by plagioclase
541 phenocrysts and rarer Ti- and Na-poor clinopyroxene (plus amphibole and quartz in the most
542 evolved products); 2) subalkaline serial affinity, with low TiO_2, MgO and alkalis, high Al_2O_3
543 and SiO_2; 3) spiked primitive mantle-normalized pattern, with peaks at U, K and Pb, troughs

at Nb and Ta, and a general LILE enrichment relative to LREE and HFSE; 4) high Ba/Nb (56-90 and 22-37, respectively for andesitic and dacitic rocks) and La/Nb (1.9-2.9 and 0.7-1.0), low Ce/Pb (3.3-4.8 and 2.7-4.8), low Nb/U (3.7-10.4 and 17.5-20.6) and low Nb/Nb* (0.1-0.3 and 0.5-0.8). The overall variations observed for mineral chemistry and whole-rock compositions could be taken as indicative that LEEM basaltic andesites, andesites and dacites are genetically linked through fractional crystallization processes. However, there are some observations that possibly argue against this.

First, the wide compositional spectrum recorded by plagioclase, as well as by clinopyroxene, amphibole and (less evidently) opaques from LEEM andesitic samples is at odds with chemical equilibrium. This is in contrast to the very homogeneous andesinic plagioclase of LEEM dacites. In particular, the composition of nearly all the analysed clinopyroxene crystals indicates disequilibrium with coexisting melt, given their much higher Mg# with respect to Mg# in the host rock [assuming equilibrium $K_D(Fe\text{-}Mg)^{cpx/melt} = 0.27 \pm 0.03$; Fig. 12a]. The presence of such kind of compositions is interpreted as the recycling of xenocryst phases crystallized from more primitive parental melts. The few equilibrium clinopyroxene crystals from LEEM andesites seem to have crystallized at ~1000-1050 °C, according to the model from Putirka (2008).

Plagioclase composition in LEEM andesites is very variable, ranging from anorthite ($An_{91.4}Ab_{8.4}Or_{0.2}$) to andesine ($An_{34.2}Ab_{62.4}Or_{3.5}$). This range is particularly wide considering that the extreme values have been measured in two andesites with nearly similar compositions (FEM14 and FEM18; ESM2.1). Wide variation of plagioclase composition can be related to variation in temperature or water content in crystallizing magma. It is well known, indeed, that plagioclases crystallized at high temperature are characterized by high anorthite content. At the same time, the more water dissolved in the melt the higher the $K_D(Ca\text{-}Na)^{pl/melt}$, resulting in Ca-rich plagioclase crystallizing in hydrous melts.

If the clinopyroxene-melt equilibrium temperatures are used, and pressure values in the 4-8 kbar range (mid-lower crust) are assumed, the Waters and Lange (2015) plagioclase-melt hygrometer indicates that LEEM andesitic magmas had 3.5-5.5 wt.% of H_2O, depending on the plagioclase-melt pair chosen. The $K_D(Ca\text{-}Na)^{pl/melt}$ is strongly dependent on the water dissolved in magma, with values close to 1 in melts with less than ~3 wt.% H_2O and values >5 in melts with more than 8 wt.% dissolved H_2O (e.g., Martel et al., 2006; Waters and Lange, 2015). On the basis of the calculated dissolved H_2O values, LEEM plagioclases should be characterized by $K_D(Ca\text{-}Na)^{pl/melt}$ ranging from 2 to 3. The extremely variable measured values for $K_D(Ca\text{-}Na)^{pl/melt)}$ (Fig. 12b) indicate that only a small fraction of these plagioclase have attained equilibrium with the melt. Interestingly, the few analysed plagioclase crystals from LEEM dacites plot very close to the $K_D(Ca\text{-}Na)^{pl/melt)} = 1$ curve, corresponding to much lower H_2O contents and therefore inconsistent with derivation from LEEM andesites via closed-system fractional crystallization.

4.2. Petrogenesis of LEEM dacites

The absence of a genetic link between LEEM andesites and dacites is also suggested by the major scattering of some of the observed trends vs. SiO_2, especially that for MgO. In fact, LEEM andesitic and dacitic rocks display basically similar MgO concentrations, which are therefore very poorly correlated with SiO_2. A better correlation is evident if the two are considered separately, with a single differentiation trend for LEEM basaltic andesites and andesites (very scattered, with R^2 ~0.25), and one for LEEM dacites (R^2 ~0.51). Attempts to modelling the andesite to dacite transition by means of mass-balance calculations, failed to successfully reproduce such evolutionary step (yielding very high values of the sum of squared residuals, typically ΣR^2 >6). In addition, the decrease of MREE and HREE contents from andesitic to dacitic rocks would require significant amphibole fractionation, which

seems inconsistent with the observed paragenesis, where only few amphibole crystals have been recognized. Finally, the only analysed dacite features an anomalous Nd-radiogenic composition (overlapping with two evolved literature samples from Agay; Beccaluva et al., 1994, 2005), coupled with the lowest $^{87}Sr/^{86}Sr$ (0.70448) among the LEEM rocks.

All these observations could be interpreted assuming that the genesis of LEEM dacites involved substantial lower crustal contamination. As interaction with such basic lithologies is likely to produce an increase of MgO and a decrease of SiO_2, it could be proposed that LEEM dacites were generated by the mixing between a lower crustal component and a (rhyolitic?) Si-rich magma, possibly cogenetic with LEEM andesites (as indicated by the comparable Sr-Pb isotope ratios). Such process would justify both the relatively high MgO (comparable with that of andesitic rocks) and the unusually low REE budget of LEEM dacites. A possible alternative model could assume that the geochemical peculiarities of LEEM dacites simply reflects the composition of a different parental melt with respect to that of LEEM andesites. This model assumes that pods of primitive basaltic melt might have interacted with harzburgitic depleted mantle domains at the top of the upper mantle, acquiring a low $^{87}Sr/^{86}Sr$ and high $^{143}Nd/^{144}Nd$ signature. Such modified melts (trapped at the mantle/crust interface due to their relatively high density) would have evolved to lower density dacitic melts, thus finally finding their way to the surface, preserving the unusual isotopic composition of the parental melts.

4.3. Mantle sources of LEEM rocks

As regards mantle source characterization, detailed comments or hypotheses are hampered due to the differentiated nature (low Mg#, Ni and Cr; lack of forsteritic olivine) even of the least evolved LEEM basaltic andesites. However, the overall homogeneity of LEEM Sr-Nd-Pb ratios might be taken to suggest that parental “primitive” basaltic melts had a similar

619 isotopic signature, which will be therefore used to make at least some general inferences on
620 the mantle source characteristics.
621 According to their isotope composition, LEEM rocks fall in the enriched field defined by
622 coeval Central-Western Mediterranean subduction-related rocks, with $^{87}Sr/^{86}Sr$ exceeding that
623 of the BSE, coupled with generally unradiogenic $^{143}Nd/^{144}Nd$ below the ChUR, except the
624 dacite with $^{143}Nd/^{144}Nd = 0.512912$. The subduction-related nature of LEEM rocks is also
625 consistent with Pb isotopic ratios, especially the relatively radiogenic $^{207}Pb/^{204}Pb$ (pointing
626 towards the EM-II mantle component). This has been related to the presence of old crustal
627 lithologies (characterised by relatively high $^{207}Pb/^{206}Pb$ due to the much shorter half-life of
628 ^{235}U compared to ^{238}U), typically reflecting a derivation from melting of the mantle wedge
629 metasomatically enriched by fluids released from the subducted oceanic lithosphere. In
630 analogy to what proposed for the genesis of "orogenic" rocks from the coeval districts, a
631 depleted MORB-like source (melting in the spinel stability facies, as indicated by HREE-
632 flattened normalized patterns), variably metasomatized by slab melts/fluids, can be envisaged
633 (e.g., Morra et al., 1997; Duggen et al., 2005; Conticelli et al., 2009; Mattioli et al., 2012;
634 Lustrino et al., 2013). It should be noted that the typical "subduction related" geochemical
635 fingerprint can be related to shallow-level magma/crust interaction too, and such open-system
636 processes surely played some role in the genesis of LEEM rocks, as reported above. However,
637 a major role of these processes seems to be ruled out considering 1) the lack of crustal
638 xenoliths/xenocrysts; 2) the typical porphyritic textures of LEEM andesites, suggesting
639 substantial fractional crystallization (where significant digestion of basement rocks would
640 rather result in vitreous to poorly-porphyritic textures; see Lustrino et al., 2013) and 3) the
641 very limited heterogeneity Sr-Nd-Pb isotope composition (with the exception of the
642 anomalously Nd-radiogenic dacite sample).
643

644 **4.4. On the "adakitic" nature of Provence "*estérellites*"**

645 The quartz-bearing microdiorites cropping out near Cap Le Dramont (St. Raphael village),
646 locally called "*estérellites*", display high SiO_2, Al_2O_3 and Na_2O/K_2O and very low HREE and
647 Y contents. All such features are usually considered the typical characteristics of adakites
648 (Defant and Drummond, 1990). However, Sr/Y (~30-58, average 40) and La/Yb (15-18,
649 average 16), though higher compared to other Provence lavas (12-21 and 4-10, respectively),
650 straddle the cut-off values with "normal" arc lavas, i.e., Sr/Y <40 and La/Yb <20. For this
651 reason, Réhault et al (2012) proposed that the Estérel microdiorites are "intermediate"
652 adakites.

653 If the term adakite is considered in its original meaning, implying derivation from melting
654 of young (and thus hot) basaltic rocks of the subducting oceanic lithosphere (Defant and
655 Drummond, 1990; Martin et al., 2005; Moyen, 2009), the Estérel microdiorites seem hard to
656 be considered true adakites. The age of the subducting oceanic lithosphere (the eastern branch
657 of the Alpine Tethys) is indeed of Jurassic age (Stampfli and Borel, 2002). However, after its
658 first definition the term adakite has been applied to rocks of extremely diverse genesis.

659 Geological contexts that are considered to allow the production of adakitic magmas include
660 1) "flat" subduction (Gutscher et al., 2000), 2) incipient subduction (e.g., Sajona et al., 1993;
661 Peacock et al., 1994), 3) "fast" subduction (e.g., Honda, 1985), 4) terminal subduction or
662 post-collisional stage (e.g., Sajona et al., 1994; Maury et al., 1996) and 5) development of a
663 slab tear or slab window (e.g., Thorkelson, 1996).

664 Martin et al. (2005) identified two distinct compositional groups of adakites based on their
665 silica content. The high-silica adakites (HSA) were considered to represent subducted basaltic
666 slab-melts that have reacted with peridotite during ascent (i.e., corresponding to "adakites"
667 *sensu* Defant and Drummond, 1990). On the other hand, the low-silica adakites (LSA) were
668 interpreted to have formed by melting of peridotitic mantle wedge whose composition has

been modified by reaction with felsic slab-melts (corresponding to the "magnesian andesites" from Adak Island, western Aleutian arc; Kay, 1978).

In more recent times, the increasing recognition of adakite-like rocks in continental collision zones (e.g., Chung et al., 2003) and extensional environments (e.g., Wang et al., 2006; Ma et al., 2012) has led to propose alternative petrogenetic models and to introduce new adakite varieties, like "C-type adakite", "continental adakite" or even the somewhat self-contradictory "potassic adakite" (Rapp et al., 2002; Xu et al., 2004; Guo et al., 2006, 2007; Zhou et al., 2006; Ding et al., 2007; Gao et al., 2007; Wang et al., 2007a,b). All these refer to any kind of intermediate or acid igneous rock whose Sr/Y is high enough to be considered "adakitic" and with chemical characteristics similar to those of adakite, but unconnected to direct slab melting. The high Sr/Y and La/Yb "adakitic" signature can be indeed produced by alternative mechanisms such as melting of a high Sr/Y crustal source at relatively low P (~5-10 kbar; Moyen, 2009), shallow depth fractionation of Sr-rich and Y-poor amphiboles, or deep level fractionation of an assemblage dominated by garnet and high pressure Mg-rich amphibole (e.g., Castillo, 2012; Ribeiro et al., 2016).

In the light of such "expanded" definition, the Estérel microdiorites might have been considered adakites generated at the initiation of subduction of relatively old oceanic crust (e.g., Sajona et al., 1993), since, according to Réhault et al. (2012), their emplacement marks the onset of subduction-related magmatic activity in the present-day Ligurian margin. However, the $^{40}Ar/^{39}Ar$ age obtained in the present study (St. Raphael dacite; 40.87 ± 0.80 Ma) does not fit the geodynamic model by Réhault et al (2012), as it shifts back the beginning of the magmatic activity in Provence to late Eocene, coherently with what proposed by Lustrino et al. (2009) studying similar and coeval rocks from NW Sardinia. This excludes that the emplacement of Estérel microdiorites marked the onset of subduction-related magmatism in the area, a consequently precludes them to be considered "adakitic".

694

695 **4.5. Origin of LEEM in the Apennine-Maghrebide subduction system framework**

696 The palinspastic reconstruction of Carminati et al. (2012) offers an alternative view to
697 explain the origin of the "subduction-related" magmatism of Provence. In a mid Eocene
698 reconstruction (45 Ma ago), the embryonic Central-Western Mediterranean had a completely
699 different aspect, with the western branch of the Alpine Tethys approaching its final
700 obliteration beneath Alpine Chain and being already completely subducted beneath the
701 AlKaPeCa block (Fig. 3 of Carminati et al., 2012). Lutetian is also the mostly likely stage that
702 marked the beginning of the Apennine-Maghrebide NW-directed subduction (Lustrino et al.,
703 2009; Carminati et al., 2010).

704 On this ground, it is not possible to link the 41-38 Ma old (or, in general, the oldest pre-
705 Chattian) igneous rocks now cropping out in Sardinia (Calabona) and Provence (St. Raphael,
706 Estérel) to the direct influence of the subducting slab on the mantle wedge. This hypothesis, at
707 least for the Eocene stage of the Eocene-Middle Miocene magmatic phase in Sardinia and
708 Corsica, is not valid, because at that time the slab had not yet reached the depths where it
709 could induce partial melting in the metasomatized mantle wedge. Moreover, the distance from
710 the front of the trench and the areas where the Late Eocene igneous activity are recorded (in
711 the order of 200-250 km) precludes any direct link between Alpine Tethys subduction and the
712 "subduction-related" igneous activity in Sardinia and Provence.

713 In other words, the first manifestations of subduction-related igneous activity in Sardinia
714 and Provence cannot have the same origin of the much more abundant Miocene igneous
715 activity. Partial melting of the over-thickened lithospheric mantle beneath Sardinia and
716 Provence, metasomatized during the previous Variscan Orogeny (e.g., Lustrino, 2000) has
717 been already proposed as a tectonic mechanism, but without any geochemical constraint
718 (Carminati et al., 2012). Here we propose the same solution, possibly validated by the

719 "adakitic" geochemical signature of the oldest samples, here interpreted not as consequence of
720 hot oceanic slab partial melting, but rather as partial melting of an ancient over-thickened
721 lithospheric mantle metasomatized during previous orogenetic cycles (i.e., Variscan
722 Orogeny). The slightly higher than usual Sr/Y ratio of the oldest and more evolved samples
723 (dacites) could reflect higher crustal input and/or interaction with lower crustal over-thickened
724 garnet-bearing lithologies. The relatively high Zr-Hf pair, testified by positive anomalies in
725 primitive mantle-normalized diagram (Fig. 9) could testify for a relatively high contribution
726 of ancient crustal zircon-rich lithologies in the sources of the most evolved and most ancient
727 igneous rocks of Provence.
728
729 **4.6. The late Miocene-Pliocene Rocks (LMP)**
730 Mineralogical (abundance of Mg-rich olivine, Ti-Na-rich clinopyroxene) and geochemical
731 constraints (SiO_2- and Al_2O_3-poor and TiO_2- and MgO-rich compositions, coupled with
732 HFSE-rich and LILE-poor compositions) indicate a completely different origin of LMP rocks
733 with respect to the LEEM group. With the exception of sample FEM31, LMP rocks have a
734 quite homogeneous composition, with geochemical signature clearly pointing to typical
735 "anorogenic" magmas, showing incompatible element content and inter-elemental
736 fractionation (e.g., peaks at Nb-Ta, low Ba/Nb = 9.7-15.3 and La/Nb = 0.6-1.3) similar to
737 those observed classical OIB. However, such homogeneity is not perfectly reflected in the
738 composition of the analysed mineral phases (see section 3.2). More specifically, both olivine
739 and clinopyroxene crystals are mostly Mg-poorer with respect to those expected to have
740 equilibrated with host magmas [assuming equilibrium $K_D(Fe\text{-}Mg)^{ol/melt}$ = 0.33 and 0.27,
741 respectively; Fig. 12a]. Also plagioclase crystals possibly bear evidences for phase/melt
742 disequilibrium, as the high $K_D(Ca\text{-}Na)^{pl/melt}$ values measured for some of these point to
743 relatively high H_2O contents (i.e., between 3 and 5 wt.%; Fig. 12b), which seem inconsistent

744 with both their weakly evolved composition and their paragenesis lacking hydrous mineral
745 phases.

746 As regards mantle source characterization, according to the experimental evidence by
747 Hirose and Kushiro (1993), which suggest that increasing melting depths in intraplate settings
748 increase FeO and decrease SiO_2 contents of mafic mantle melts, LMP magmas seem to have
749 generated at relatively low depths (between 33 and 66 km). The relatively high MREE/HREE
750 of LMP magmas (Dy_N/Yb_N = 1.77-1.98), however, points to the presence of residual garnet in
751 the mantle source. Therefore, given that the spinel/garnet transition in mantle peridotites is
752 inferred to occur at ~70-80 km (extending to much higher depths in cold geotherm regimes;
753 Ziberna et al., 2013), it is proposed that LMP magmas were generated approximately in a
754 garnet/spinel facies mantle, with higher amounts of garnet. The mantle source would be likely
755 located just below the shallower metasomatized sub-continental lithosphere that generated the
756 "orogenic" LEEM magmas.

757 From a Sr-Nd point of view LMP rocks fall in the depleted isotopic field, with
758 unradiogenic $^{87}Sr/^{86}Sr$, below the BSE, and radiogenic $^{143}Nd/^{144}Nd$, above ChUR, largely
759 overlapping with the isotopic ranges of the coeval "anorogenic" rocks of Languedoc, Spain
760 and RPV rocks of Sardinia. Such compositions are largely represented in the rocks of the
761 CiMACI province (Lustrino and Wilson, 2007), with the only exception being represented by
762 the UPV Sardinia rocks. The Sr-Nd isotope ratios of LMP rocks (as well as that of the other
763 CiMACI rocks) point towards the HIMU end-member and the FOZO (Focus Zone)
764 component, both essentially present in rocks from intraplate settings (Stracke et al., 2005) and
765 substantially absent in "subduction-related" magmas. In addition, Pb isotopes suggest mixing
766 between HiMu-OIB (i.e., high $^{206}Pb/^{204}Pb$, low $^{207}Pb/^{206}Pb$ and $^{208}Pb/^{206}Pb$) and EM-II mantle
767 components (high $^{207}Pb/^{204}Pb$ and $^{207}Pb/^{206}Pb$). Both the hypothetical mantle end-members
768 (HiMu and EM-II) are ultimately related to the presence of olivine-poor lithologies (eclogites

769 to garnet-pyroxenites and olivine websterites). The substantial similarity with other CiMACI
770 rocks, for which numerous evidences have been provided against a plume-origin (e.g.,
771 Duggen et al., 2005; Lustrino and Wilson, 2007; Lustrino et al., 2007, 2011, 2013), suggests
772 derivation from a common source, without any necessary link with deep mantle dynamics.
773 The EM-II component is thought to reflect the involvement of terrigenous sediments in
774 mantle sources or some interaction with local upper crust.

775 The geochemical peculiarities of FEM31 sample (e.g., notably lower TiO_2, K_2O, Sr, Cr and
776 Ni, higher Al_2O_3, MgO, and CaO; primitive mantle-normalized pattern with troughs at Nb-Ta
777 and Ba, Cs enrichment and low L-MREE/HREE) require a substantially different petrogenetic
778 model with respect to the above LMP basalts. However, the lack of isotope data for this
779 sample hampers a detailed treatment of this issue. It could be speculated that its anomalous
780 composition could be either related to shallow depth crustal contamination (consistent with
781 the above evidences for the presence of crystal phases clearly out of equilibrium), or to the
782 derivation from a mantle source retaining crustal input of the previous orogenetic phases. In
783 addition, it should be observed that the close spatial and temporal association with the LEEM
784 "orogenic" magmas could have resulted in some occasional interaction between LMP
785 asthenospheric melts with portions of (or melts from) the metasomatized sub-continental
786 lithospheric mantle, the source for the LEEM. This is definitely not uncommon for the
787 Cenozoic districts of the Central-Western Mediterranean where a similar transition in magma
788 types is recorded (i.e., Sardinia, Spain, Morocco, Serbia, Pannonian Basin and Turkey; see
789 Lustrino and Wilson, 2007, and references therein).

790

791 **4.7. Petrological and geotectonic implications**

792 As previously outlined, the Cenozoic igneous activity of Provence is strictly linked with
793 the geodynamic evolution of the Central-Western Mediterranean area, as it is also evident

794 from the overall petrochemical similarities of the outcropping igneous rocks. However, the
795 volume of Provence rocks is about three orders of magnitude smaller than that of coeval
796 products of Sardinia, a characteristic that is likely related to the much lower stretching rates
797 that characterised Provence due to its proximity to the rotation hinge of the Sardinia-Corsica
798 block (Gattacceca et al., 2007).

799 The new $^{40}Ar/^{39}Ar$ age data for the Estérel dacite presented here (~41 Ma) allows shifting
800 back the beginning of the "subduction-related" igneous activity to late Eocene. This late
801 Eocene-early Miocene magmatic cycle, roughly contemporaneous with those developed in
802 Sardinia (~38-15 Ma ago; Lustrino et al., 2009) and southern Spain (~38-6 Ma ago; Turner et
803 al., 1999 and Duggen et al., 2004), is classically believed to represent the effect of the NW-
804 directed subduction system that involved the recycling of the Neo-Tethyan oceanic
805 lithosphere beneath the southern European paleo-margin.

806 Lustrino et al (2009) proposed that the beginning of NW-directed Apennine subduction
807 responsible for the subduction-related late Eocene-middle Miocene igneous activity of
808 Sardinia, occurred between ~49 and ~42 Ma ago, more or less in concomitance with the
809 emplacement of the Periadriatic Magmatic province in the Alps (~42 Ma ago). The early
810 "orogenic" magmatism took place along the paleo-European-Iberian continental margin, and
811 developed with arc-tholeiitic/calcalkaline magmatism in Sardinia, Provence and in the Betic
812 Cordillera. However, the new ~41 Ma $^{40}Ar/^{39}Ar$ age obtained for the St. Raphael dacite would
813 shift back of the beginning of the Apennine subduction of several million of years.

814 Following Lustrino et al. (2009), assuming a slab dip of 45°, upper and lower plate
815 convergence at 1-3 cm/yr rate and dehydration of amphibole occurring between ~80 and 120
816 km, the beginning of the Apennine subduction would have started at least in the early Eocene
817 (~52-53 Ma ago). Lustrino et al. (2013) emphasized the problem represented by the horizontal
818 distance of the volcanic arc from the subduction hinge, which had not been addressed in the

819 previous models. On this grounds, the authors proposed that the earliest subduction-related
820 igneous manifestations in the Central-Western Mediterranean area (dated ~38-23 Ma ago) are
821 not related with the metamorphic dehydration of the subducted Alpine Tethys, but rather to
822 the pushing effects of the subducting slab over the ancient lower crust of the overriding
823 European plate. Hence, the subduction-related signature of the early igneous activity of
824 Provence (and Sardinia) might either reflect an ancient mantle modification (likely occurred
825 during the Variscan Orogeny), or might be related to the partial melting of the Variscan lower
826 crust.

827 The production of "anorogenic" magmas shortly after the end of "orogenic" magmatic
828 activity, quite common in the Cenozoic districts of the Central-Western Mediterranean area
829 (e.g., Lustrino et al., 2011 and references therein) might have been triggered by the roll-back
830 and steepening of the subducted Tethys oceanic lithosphere, causing delamination/detachment
831 of the sub-continental mantle lithosphere (mechanically coupled to the subducting slab) and
832 passive upwelling of the asthenospheric mantle. In some instances this model is further
833 validated by the observation that magmas from the two phases, notwithstanding their
834 remarkably contrasting geochemical signatures, were produced at largely similar depths (e.g.,
835 southern Spain and Northern Morocco; Duggen et al., 20005). Although LEEM and LMP
836 magmas seem to have originated at different depths (i.e., respectively within the spinel- and
837 garnet-bearing facies), the striking similarity with their counterparts from the coeval
838 neighbouring districts makes it unlikely that the "orogenic" to "anorogenic" transition in
839 Provence was related to a different process.

840 As a final remark, it should be observed that if the Sardinia-Corsica block is restored to its
841 position preceding its counter-clockwise rotation, the LMP rocks were emplaced in an area
842 that was linked with northern Sardinia, where coeval magmatism produced the "unusual"
843 UPV rocks with unique isotopic signature within the entire CiMACI province. The

844 occurrence of the UPV rocks has been ascribed to the existence of a lithospheric discontinuity
845 running roughly E-W in southern Sardinia, separating the "normal" (i.e., CiMACI-like) RPV
846 source to the South, from the "peculiar" UPV source, modified by ancient interaction with
847 lower crust, to the North (Lustrino et al., 2007a). Therefore, the isotopic similarity between
848 Provence LMP and Sardinia RPV rocks can be taken to suggest that an additional lithospheric
849 discontinuity should be postulated, running approximately N-S along present-day Sardinia
850 western coast.
851

852 ## 5. Conclusions

853 The Cenozoic igneous activity in Provence mainly emplaced microdiorites, basalts,
854 basaltic andesites, andesites and dacites during two completely distinct igneous phases. The
855 first phase occurred during the late Eocene-early Miocene time span and emplaced
856 intermediate and evolved andesitic to dacitic rocks, with low TiO_2 and generally high Al_2O_3
857 and CaO, and a calcalkaline to arc-tholeiitic serial affinity. Magma evolution occurred not
858 only via fractional crystallization but also involved some shallow-level crustal assimilation
859 and the interaction with the lower crust or with harzburgitic domains at the mantle/crust
860 interface.
861 The LEEM rocks display a significant LILE/HFSE enrichment, with a composition
862 resembling that of coeval subduction-related products from the neighbouring areas. The Sr-
863 Nd-Pb isotopic composition of LEEM rocks suggest the involvement of a shallow sub-
864 continental lithosphere mantle source variably modified by slab-derived components. The
865 definition of the Ligurian-Provençal Basin as a classical "back-arc" basin should be replaced
866 to "intra-arc" basin, because of the presence of the same type of coeval igneous rocks on both
867 shoulders of the Ligurian-Provençal Basin.

The second igneous phase occurred in the late Miocene-Pliocene time span (LMP) and emplaced basalts with high MgO and TiO_2 and Na-alkaline serial affinity. These rocks mark the transition from the previous subduction-related LEEM activity to an "anorogenic" magmatism, a feature that is common for many other Cenozoic igneous districts of the Central-Western Mediterranean area. The isotopic composition of LMP rocks is consistent with derivation from a sub-lithospheric mantle source, approximately located at the spinel/garnet transition boundary, with HiMu (i.e., involving recycled lithologies) and EM-II (involving terrigenous sediments or interaction with local upper crust) compositions. Additional processes such as shallow-level crustal contamination or the introduction of subducted sediments or fluids into the mantle source, or even interaction with LEEM source/melts were also active, as indicated by the sporadic occurrence of "anomalous" compositions (e.g., relatively low TiO_2 and Nb, mantle-normalized patterns with Nb-Ta and Ba troughs observed in sample FEM31).

The new $^{40}Ar/^{39}Ar$ data allow us to shift back the beginning of the first igneous phase of Provence at ~41 Ma ago, ~7 Ma earlier than previously thought, and to shift forward the last manifestations of the second igneous phase to ~5.6 Ma ago, up to ~1 Ma earlier than previously known. The first could imply that also the beginning of the NW-directed subduction beneath the southern European paleo-margin should be moved back. This possibility seems however unlike, as only sporadic igneous activity is recorded in Central-Western Mediterranean area in the late Eocene. Therefore, following Carminati et al. (2012) and Lustrino et al (2013), the earliest subduction-related igneous phases are here considered related to the pushing effects of the subducting Alpine Tethys over the ancient lower crust of the overriding plate, rather than to the dehydration of the subducting slab and the associated melting of the mantle wedge. This also excludes the postulated "adakitic" nature of the

892 Provence microdiorites ("*estérellites*"), emplaced at ~34 Ma ago and classically considered to
893 mark the onset of subduction-related magmatism in Provence.
894

895 ## Acknowledgements

896 ML thanks, as usual, Enrica, Bianca and Laura for the patience during all the stages of data
897 collection and manuscript preparation and Marcello Serracino for his skill in maintaining
898 perfectly working the microprobe. ML thanks also Geddy Lee, Alex Lifeson, and Neil Peart
899 for the warm hospitality in La Villa Strangiato. Data processing was mostly done using the
900 free Petroplot software by Yongjun Su, Charles H. Langmuir and Paul D. Asimow and
901 clinopyroxene classification was done using PX-NOM software by R. Sturm. Silvio Mollo
902 (Rome) is thanked for discussion on mineral-melt equilibria. Stefano Piasentin and Luigi
903 Antonaci are thanked for the contribution during the first stages of data processing. This study
904 benefitted of Sapienza Università di Roma (Fondi Ateneo, 2013, 2014, 2015) financial
905 support.
906

907 **Electronic Supplementary Material 1**: analytical techniques and sources for the
908 bibliographic data for the coeval Cenozoic igneous rocks from the neighbouring districts of
909 Sardinia, Alps, N-Apennines, Corsica-Estérel, Spain and Languedoc used in the presented
910 diagrams.
911 **Electronic Supplementary Material 2**: full analytical datasets (mineral chemistry, $^{40}Ar/^{39}Ar$,
912 whole-rock and Sr-Nd-Pb isotopic data) for the investigated Cenozoic igneous rocks from
913 Provence.
914 **Electronic Supplementary Material 3**: major element (plus CaO/Al_2O_3) binary variation
915 diagrams for the rocks of the two Cenozoic igneous cycles of Provence (LEEM and LMP) not
916 included in Fig. 7. Symbols and literature data as in Fig. 5.

Electronic Supplementary Material 4: trace element binary variation diagrams for the rocks of the two Cenozoic igneous cycles of Provence (LEEM and LMP) not included in Fig. 8. Symbols and literature data as in Fig. 5.

Electronic Supplementary Material 5: $^{87}Sr/^{86}Sr$ (**a**) and $^{143}Nd/^{144}Nd$ (**b**) vs. SiO_2 diagrams for the rocks of the two Cenozoic igneous cycles of Provence (LEEM and LMP). Symbols and literature data as in Fig. 5.

Electronic Supplementary Material 6: $^{206}Pb/^{204}Pb$ (**a**), $^{207}Pb/^{204}Pb$ (**b**) and $^{208}Pb/^{204}Pb$ (**c**) vs. SiO_2 diagrams for the rocks of the two Cenozoic igneous cycles of Provence (LEEM and LMP). Symbols and literature data as in Fig. 5.

References

Arculus, R.J., 2003. Use and abuse of the terms calcalkaline and calcalkalic. Journal of Petrology 44, 929-935.

Argnani, A., Cimini, G.B., Frugoni, F., Monna, S., Montuori, C., 2016. The role of continental margins in the final stages of arc formation: constraints from teleseismic tomography of the Gibraltar and Calabrian Arc (Western Mediterranean). Tectonophysics 677-678, 135-152.

Baubron, J.C., 1974. Etude de l'évolution magmatique des formations calco-alcalines tertiaries de Provence et Haute-Provence par la géochimie du rubidium et du strontium. Raport de Bureau de Recherches Géologiques et Minières 74, Service Géologique National 003 LAB, 37 pp.

Beccaluva, L., Bigioggero, L.B., Chiesa, S., Colombo, A., Fanti, G., Gatto, G.O., Gregnanin, A., Montrasio, A., Piccirillo, E.M., Tunesi, A., 1983. Postcollisional orogenic dyke magmatism in the Alps. Memorie della Società Geologica Italiana 26, 341-359.

Beccaluva, L., Civetta, L., Macciotta, G., Ricci, C.A., 1985. Geochronology in Sardinia: results and problems. Rendiconti della Società Italiana di Mineralogia e Petrologia 40, 57-72.

941 Beccaluva, L., Coltorti, M., Galassi, B., Macciotta, G., Siena, F., 1994. The Cainozoic calcalkaline
942 magmatism of the western Mediterranean and its geodynamic significance. Bollettino di Geofisica
943 Teorica ed Applicata 36, 293-309.
944 Beccaluva, L., Bianchini, G., Coltorti, M., Siena, F., Verde, M., 2005. Cenozoic tectono-magmatic
945 evolution of the central-western Mediterranean: migration of an arc-interarc basin system and
946 variations in the mode of subduction. CROP Project: Deep seismic exploration of the central
947 Mediterranean and Italy 623-639.
948 Beccaluva, L., Bianchini, G., Mameli, P., Natali, C., 2013. Miocene shoshonite volcanism in
949 Sardinia: implications for mantle sources and geodynamic evolution of the central-western
950 Mediterranean. Lithos 180-181, 128-137.
951 Belayouni, H., Brunelli, D., Clocchiatti, R., Di Staso, A., El Amrani El Assani, I.-E., Guerrera, F.,
952 Kassaa, S., Ouazaa, N.L., Martín Martín, M., Serrano, F., Tramonana, M., 2010. La Galite
953 Archipelago (Tunisia, North Africa): stratigraphic and petrographic revision and insights for
954 geodynamic evolution of the Maghrebian Chain. Journal of African Earth Sciences 56, 15-28.
955 Bellon, H., 1981. Chronologie radiométrique (K–Ar) desmanifestationsmagmatiques atout de la
956 Méditerranée occidentale entre 33 et 1 Ma. In: Wezel, F.C. (Ed.), Sedimentary basins of
957 Mediterranean margins. Tecnoprint, Bologna, Italy, pp. 341-360.
958 Bellon, H., Brousse, R., 1971. L'âge oligo-miocène du volcanisme ligure. Comptes Rendus de
959 l'Académie des Sciences de Paris 272, 3109-3111.
960 Bellon, H., Bordet, P., Montenat, C., 1983. Chronologie du magmatisme Néogène des Cordillères
961 Bétiques, Espagne méridionale. Bulletin de la Société Géologique de France 25, 205-217.
962 Bestani, L., Espurt, N., Lamarche, J., Floquet, M., Philip, J., Bellier, O., Hollender, F., 2015. Structural
963 style and evolution of the Pyrenean-Provence thrust belt, SE France. Bulletin de la Société
964 Géologique France 186, 223-241.

965 Blundell, D., Freeman, R., Mueller, S., 1992. A Continent Revealed, The European Geotraverse.
966 Cambridge University Press, Cambridge, 276 pp.
967 Bouillin, J. P., Durand-Delga, M., Olivier, P., 1986. Betic-Rifian and Tyrrhenian arcs: distinctive
968 features, genesis and development stages. In: Wezel, F.-C. (Ed.), The origin of arcs 21, 281-304.
969 Carmichael, I.S.E., 1967. The iron-titanium oxides of salic volcanic rocks and their associated
970 ferromagnesian silicates. Contributions to Mineralogy and Petrology 14, 36-64.
971 Carminati, E., Lustrino, M., Cuffaro, M., Doglioni, C., 2010. Tectonics, magmatism and geodynamics of
972 Italy: what we know and what we imagine. Journal of the Virtual Explorer 36, paper 9,
973 http://dx.doi.org/10.3809/jvirtex.2010.00226
974 Carminati, E., Lustrino, M., Doglioni, C., 2012. Geodynamic evolution of the central and western
975 Mediterranean: Tectonics vs. igneous petrology constraints. Tectonophysics 579, 173-192.
976 Casciello, E., Fernàndez, M., Vergés, J., Cesarano, M., Torne, M., 2015. The Alboran domain
977 in the western Mediterranean evolution: the birth of a concept. Bulletin de la Société
978 Géologique de France 186, 371-384.
979 Castillo, P.R., 2012. Adakite petrogenesis. Lithos 134-135, 304-316.
980 Cebrià, J.M., Lopez-Ruiz, J., Carmona, J., Doblas, M., 2009. Quantitative petrogenetic constraints on the
981 Pliocene basaltic volcanism of the SE Spain Volcanic Province. Journal of Volcanology and
982 Geothermal Research 185, 172-180.
983 Champion, C., Choukroune, P., Clauzon, G., 2000. La déformation post-Miocène en Provence
984 occidentale. Geodinamica Acta 13, 67-85.
985 Chung, S.-L., Liu, D., Ji, J., Chu, M.-F., Lee, H.-Y., Wen, D.-J., Lo, C.-H., Lee, T.-Y., Qian, Q., Zhang,
986 Q., 2003. Adakites from continental collision zones: melting of thickened lower crust beneath
987 southern Tibet. Geology 31, 1021-1024.

988 Combes, P., 1984. La tectonique récente de la Provence occidentale microtectonique, caractéristiques
989 dynamiques et cinématiques: méthodologie de zonation tectonique et relations avec la séismicité.
990 Doctoral Dissertation Thesis, Université de Strasbourg.
991 Conte, A.M., Palladino, D.M., Perinelli, C., Argenti, E., 2010. Petrogenesis of the high-alumina basalt-
992 andesite suite from Sant'Antioco Island, SW Sardinia, Italy. Periodico di Mineralogia 79, 27-55.
993 Conticelli, S., D'Antonio, M., Pinarelli, L., Civetta, L, 2002. Source contamination and mantle
994 heterogeneity in the genesis of Italian potassic and ultrapotassic volcanic rocks: Sr-Nd-Pb isotope
995 data from Roman Province and Southern Tuscany. Mineralogy and Petrology 74, 189-222.
996 Conticelli, S., Guarnieri, L., Farinelli, A., Mattei, M., Avanzinelli, R., Bianchini, G., Boari, E.,
997 Tommasini, S., Tiepolo, M., Prelević, D., Venturelli, G., 2009. Trace elements and Sr-Nd-Pb isotopes
998 of K-rich, shoshonitic, and calc-alkaline magmatism of the Western Mediterranean Region: genesis
999 of ultrapotassic to calc-alkaline magmatic associations in a post-collisional geodynamic setting.
1000 Lithos 107, 68-92.
1001 Cushing, E.M., Bellier, O., Nechtschein, S., Sébrier, M., Lomax, A., Volant, P., Bove, L., 2008. A
1002 multidisciplinary study of a slow-slipping fault for seismic hazard assessment: the example of the
1003 Middle Durance Fault (SE France). Geophysical Journal International 172, 1163-1178.
1004 Dautria, J.-M., Liotard, J.-M., Bosch, D., Alard, O., 2010. 160 Ma of sporadic basaltic activity on the
1005 Languedoc volcanic line (Southern France): A peculiar case of lithosphere-asthenosphere interplay.
1006 Lithos 120, 202-222.
1007 Defant, M.J., Drummond, M.S., 1990. Derivation of some modern arc magmas by melting of young
1008 subducted lithosphere. Nature 347, 662-665.
1009 Dercourt, J., Zonenshain, L.P., Ricou, L.E., Kazmin, V.G., le Pichon, X., Knipper, A.L., Grandjacquet,
1010 C., Sbortshikov, I.M., Geyssant, J., Lepvrier, C., Pechersky, D.H., Boulin, J., Sibuet, J.C., Savostin,
1011 L.A., Sorochtin, O., Westphal, M., Bazhenov, M.L., Lauer, J.P., Biju-Duval, B., 1986. Geological

1012 evolution of the Tethys belt from the Atlantic to the Pamirs since the Lias. Tectonophysics 123, 241-
1013 315.
1014 Ding, L., Kapp, P., Yue, Y., Lai, Q., 2007. Postcollisional calc-alkaline lavas and xenoliths from the
1015 Southern Qiangtang terrane, central Tibet. Earth and Planetary Science Letters 254, 28-38.
1016 Doglioni, C., 1991. A proposal of kinematic modelling for W-dipping subductions - possible
1017 applications to the Tyrrhenian-Apennines system. Terra Nova 3, 423-434.
1018 Doglioni, C., Mongelli, F., Pialli, C., 1998. Boudinage of the Alpine Belt in the Apenninic back-arc.
1019 Memorie della Società Geologica Italiana 52, 457-468.
1020 Doglioni, C., Gueguen, E., Harabaglia, P., Mongelli, F., 1999. On the origin of W-directed subduction
1021 zones and applications to the western Mediterranean. Geological Society of London Special
1022 Publication 156, 541-561.
1023 Duggen, S., Hoernle, K., van den Bogaard, P., Harris, C., 2004. Magmatic evolution of the Alborán
1024 region: the role of subduction in forming the western Mediterranean and causing the Messinian
1025 salinity crisis. Earth and Planetary Science Letters 218, 91-108.
1026 Duggen, S., Hoernle, K., van den Bogaard, P., Garbe-Schonberg, D., 2005. Post-collisional transition
1027 from subduction- to intraplate-type magmatism in the westernmost Mediterranean: evidence for
1028 continental-edge delamination of subcontinental lithosphere. Journal of Petrology 46, 1155-1201.
1029 Elter, F.M., Corsi, B., Cricca, P., Muzio, G., 2004. The south-western Alpine foreland: correlation
1030 between two sectors of the Variscan chain belonging to "stable Europe": Sardinia-Corsica and the
1031 Maures Massif (south-eastern France). Geodinamica Acta 17, 31-40.
1032 Elter, F.M., Pandeli, E., 2005. Structural-metamorphic correlations between three Variscan segments in
1033 Southern Europe: Maures Massif (France), Corsica (France)-Sardinia (Italy), and Northern
1034 Appennines (Italy). Journal of the Virtual Explorer 19, paper 1.
1035 Faccenna, C., Becker, T.W., Auger, L., Billi, A., Boschi, L., Brun, J.P., Capitanio, F.A.,
1036 Funiciello, F., Horvàth, F., Jolivet, L., Piromallo, C., Royden, L., Rossetti, F., Serpelloni,

1037 E., 2014. Mantle dynamics in the Mediterranean. Review of Geophysics 52,
1038 doi:10.1002/2013RG000444
1039 Faccenna, C., Mattei, M., Funiciello, R., Jolivet, L., 1997. Styles of back-arc extension in the central
1040 Mediterranean. Terra Nova 9, 126-130.
1041 Féraud, G., Ruffet, G., Stéphan, J.F., Lapierre, H., Delgado, E., Popoff, M., 1996. Nouvelles données
1042 géochronologiques sur le volcanisme paléogène des Alpes occidentales: existence d'un événement
1043 magmatique bref généralisé. In: Magmatismes dans le Sud-Est de la France, Séance Spécialisee de la
1044 Société Gèologique de France et de l'Association des Geologues du Sud-Est, p. 38.
1045 Gasperini, D., Blichert-Toft, J., Bosch, D., Del Moro, A., Macera, P., Telouk, P., Albarède, F., 2000.
1046 Evidence from Sardinian basalt geochemistry for recycling of plume heads into the Earth's mantle.
1047 Nature 408, 701-704.
1048 Gattacceca, J., Deino, A., Rizzo, R., Jones, D.S., Henry, B., Beaudoin, B., Vedeboin, F., 2007. Miocene
1049 rotation of Sardinia: new paleomagnetic and geochronological constraints and geodynamic
1050 implications. Earth and Planetary Science Letters 258, 359-377.
1051 Gao Y., Hou, Z., Kamber, B.S., Wei, R., Meng, X., Zhao, R., 2007. Adakite-like porphyries from the
1052 southern Tibetan continental collision zones: evidence for slab melt metasomatism. Contributions to
1053 Mineralogy and Petrology 153, 105-120.
1054 Guarino, V., Fedele, L., Franciosi, L., Lonis, R., Lustrino, M., Marrazzo, M., Melluso, L., Morra, V.,
1055 Rocco, L., Ronga, F., 2011. Mineral compositions and magmatic evolution of the calcalkaline rocks
1056 of northwestern Sardinia, Italy. Periodico di Mineralogia 80, 517-545.
1057 Gueguen, E., Doglioni, C., Fernandez, M., 1998. On the post 25 Ma geodynamic evolution of the
1058 western Mediterranean. Tectonophysics 298, 259-269.
1059 Guerrera, F., Martin-Algarra, A., Perrone, V., 1993. Late Oligocene–Miocene syn- late-orogenic
1060 successions in Western and Central Mediterranean Chains from the Betic Cordillera to the Southern
1061 Apennines. Terra Nova 5, 525-44.

1062 Guo, F., Fan, W., Li, C., 2006. Geochemistry of late Mesozoic adakites from the Sulu belt, eastern
1063 China: magma genesis and implications for crustal recycling beneath continental collisional orogens.
1064 Geological Magazine 143, 1-13.
1065 Guo, Z., Wilson, M., Liu, J., 2007. Post-collisional adakites in South Tibet: products of partial melting of
1066 subduction-modified lower crust. Lithos 96, 205-224.
1067 Gutscher, M.A., Maury, R.C., Eissen, J.-P., Bourdon, E., 2000. Can slab melting be caused by flat
1068 subduction? Geology 28, 535-538.
1069 Handy, M.R., Schmid, S.M., Bousquet, R., Kissling, E., Bernoulli, D., 2010. Reconciling plate tectonic
1070 reconstructions of Alpine Tethys with the geological–geophysical record of spreading and subduction
1071 in the Alps. Earth-Science Reviews 102, 121-158.
1072 Hirose, K., Kushiro, I., 1993. Partial melting of dry peridotites at high pressures: determination of
1073 compositions of melts segregated from peridotite using aggregates of diamond. Earth and Planetary
1074 Science Letters 114, 477-489.
1075 Honda, S., 1985. Thermal structure beneath Tohoku, northeast Japan. A case study for understanding the
1076 detailed thermal structure of the subduction zone. Tectonophysics 112, 69,102.
1077 Irvine, T., Baragar, W., 1971. A guide to the chemical classification of the common volcanic rocks.
1078 Canadian Journal of Earth Sciences 8, 523-548.
1079 Ivaldi, J. P., Bellon, H., Guardia, P., Mangan, C., Müller, C., Perez, J. L., Terramorsi, S., 2003. Contexte
1080 lithostructural, âges 40 K-40 Ar et géochimie du volcanisme calco-alcalin tertiaire de Cap-d'Ail dans
1081 le tunnel ferroviaire de Monaco. Comptes Rendus Geosciences 335, 411-421.
1082 Jourdon, A., Rolland, Y., Petit, C., Bellahsen, N., 2014. Style of Alpine tectonic deformation in the
1083 Castellane fold-and-thrust belt (WS Alps, France): insights from balanced cross-sections.
1084 Tectonophysics 633, 143-155.
1085 Kastens, K., Mascle, J., Auroux, C., Bonatti, E., Broglia, C., Channell, J., Curzi, P., Emeis, K.-C.,
1086 Claçon, G., Hasegawa, S., Kieke, W., Mascle, G., McCoy, F., McKenzie, J., Mendelson, J., Muller,

C., Réhault, J.-P., Robertson, A., Sartori, R., Sprovieri, R., Torii, M., 1988. ODP Leg 107 in the Tyrrhenian Sea: Insights into passive margin and back-arc basin evolution. Geological Society of America Bulletin 100, 1140-1156.

Kawabata, H., Hanyu, T., Chang, Q., Kimura, J.I., Nichols, A.R., Tatsumi, Y., 2011. The petrology and geochemistry of St. Helena alkali basalts: evaluation of the oceanic crust-recycling model for HIMU OIB. Journal of Petrology 52, 791-838.

Kay, R.W., 1978. Aleutian magnesian andesites: melts from subducted Pacific Ocean crust. Journal of Volcanology and Geothermal Research 4, 117-132.

Kelley, S., 2002. Excess argon in K-Ar and Ar-Ar geochronology. Chemical Geology 188, 1-22.

Lacombe, O., Jolivet, L., 2005. Structural and kinematic relationships between Corsica and the Pyrenees-Provence domain at the time of the Pyrenean orogeny. Tectonics 24, TC1003, doi:10.1029/2004TC001673

Lacombe, O., Angelier, J., Laurent, P., 1992. Determining paleostress orientations from faults and calcite twins: a case study near the Sainte-Victoire Range (southern France). Tectonophysics 201, 141-156.

Le Maitre, R.W., 2002. Igneous Rocks: A Classification and Glossary of Terms. Recommendations of the International Union of Geological Sciences Subcommission on the Systematics of Igneous Rocks, Cambridge University Press, Cambridge, UK, 256 p.

Leake, B.E., Woolley, A.R., Arps, C.E.S., Birch, W.D., Gilbert, M.C., Grice, J.D., Hawthorne, F.C., Kato, A., Kisch, H.J., Krivovichev, V.G., Linthout, K., Laird, J., Mandarino, J., Maresch, W.V., Nickel, E.H., Schumacher, J.C., Smith, D.C., Stephenson, N.C.N., Ungaretti, L., Whittaker, E.J.W., Youzhi, G., 1997. Nomenclature of amphiboles: report of the subcommittee on amphiboles of the International Mineralogical Association Commission on the New Minerals and Mineral Names. Mineralogical Magazine 61, 295-321.

1111 Lecca, L., Lonis, R., Luxoro, S., Melis, E., Secchi, F., Brotzu, P., 2007. Oligo-Miocene
1112 volcanic sequences and rifting stages in Sardinia: a review. Periodico di Mineralogia 66, 7-
1113 61.
1114 Lustrino, M., 2000. Phanerozoic geodynamic evolution of the Circum-Italian Realm.
1115 International Geology Reviews 42, 724-757.
1116 Lustrino, M., Anderson, D.L., 2015. The mantle isotopic printer: Basic mantle plume geochemistry for
1117 seismologists and geodynamicists. Geological Society of America Special Paper 514, 257-279.
1118 Lustrino, M., Dallai, L., 2003. On the origin of EM-I end-member. Neues Jahrbuch für
1119 Mineralogie Abhandlungen 179, 85-100.
1120 Lustrino, M., Wilson, M., 2007. The circum-Mediterranean anorogenic Cenozoic igneous province.
1121 Earth-Science Reviews 81, 1-65.
1122 Lustrino, M., Melluso, L., Morra, V., 2000. The role of lower continental crust and lithospheric mantle in
1123 the genesis of Plio-Pleistocene volcanic rocks from Sardinia (Italy). Earth and Planetary Science
1124 Letters 180, 259-270.
1125 Lustrino, M., Morra, V., Melluso, L., Brotzu, P., d'Amelio, F., Fedele, L., Franciosi, Lonis, R., Petteruti
1126 Liebercknecht, A.M., 2004. The Cenozoic igneous activity of Sardinia. Periodico di Mineralogia 73,
1127 105-134.
1128 Lustrino, M., Melluso, L., Morra, V., 2007a. The geochemical peculiarity of "Plio-Quaternary" volcanic
1129 rocks of Sardinia in the circum-Mediterranean area. In: Beccaluva, L., Bianchini, G., Wilson, M.
1130 (Eds.), Cenozoic Volcanism in the Mediterranean Area. Geological Society of America Special
1131 Paper 418, 277-301.
1132 Lustrino, M., Morra, V., Fedele, L., Serracino, M., 2007b. The transition between "orogenic" and
1133 "anorogenic" magmatism in the western Mediterranean area: the Middle Miocene volcanic rocks of
1134 Isola del Toro (SW Sardinia, Italy). Terra Nova 19, 148-159.

1135 Lustrino, M., Morra, V., Fedele, L., Franciosi, L., 2009. The beginning of the Apennine subduction
1136 system in central-western Mediterranean: constraints from Cenozoic "orogenic" magmatic rocks of
1137 Sardinia (Italy). Tectonics 28, TC5016, doi:10.1029/ 2008TC002419
1138 Lustrino, M., Duggen, S., Rosenberg, C.L., 2011. The Central-Western Mediterranean: anomalous
1139 igneous activity in an anomalous collisional tectonic setting. Earth-Science Reviews 104, 1-40.
1140 Lustrino, M., Fedele, L., Melluso, L., Morra, V., Ronga, F., Geldmacher, J., Duggen, S., Agostini, S.,
1141 Cucciniello, C., Franciosi, L., Meisel, T., 2013. Origin and evolution of Cenozoic magmatism of
1142 Sardinia (Italy). A combined isotopic (Sr-Nd-Pb-O-Hf-Os) and petrological view. Lithos 180, 138-
1143 158.
1144 Lyubetskaya, T., Korenaga, J., 2007. Chemical composition of Earth's primitive mantle and its variance:
1145 1. Method and results. Journal of Geophysical Research 112, B03211, doi:10.1029/2005JB004223
1146 Ma, Q., Zheng, J., Griffin, W.L., Zhang, M., Tang, H., Su, Y., Ping, X., 2012. Triassic "adakitic" rocks
1147 in an extensional setting (North China): Melts from the cratonic lower crust. Lithos 149, 159-173.
1148 Martel, C., Ali, A.R., Poussineau, S., Gourgaud, A., Pichavant, M., 2006. Basalt-inherited microlites in
1149 silicic magmas: evidence from Mount Pelée (Martinique, French West Indies). Geology 34, 905-908.
1150 Martin, H., Smithies, R.H., Rapp, R., Moyen, J.F., Champion, D., 2005. An overview of adakite,
1151 tonalite-trondhjemite-granodiorite (TTG), and sanukitoid: relationships and some implications for
1152 crustal evolution. Lithos 79, 1-24.
1153 Mattioli, M., Lustrino, M., Ronca, S., Bianchini, G., 2012. Alpine subduction imprint in Apennine
1154 volcaniclastic rocks. Geochemical-petrographic constraints and geodynamic implications from Early
1155 Oligocene Aveto-Petrignacola Formation (N Italy). Lithos 134-135, 201-220.
1156 Maury, R., Sajona, F.G., Pubellier, M., Bellon, H., Defant, M.J., 1996. Fusion de la croûte océanique
1157 dans les zones de subduction/collision récentes: l'exemple de Mindanao (Philippines). Bulletin de la
1158 Société Géologique de France 167, 579-595.

1159 Michard, A., Chalouan, A., Feinberg, H., Goffé, B., Montigny, R., 2002. How does the Alpine belt end
1160 between Spain and Morocco? Bulletin de la Société Géologique de France 173, 3-15.
1161 Miyashiro, A., 1974. Volcanic rock series in island arcs and active continental margins. American
1162 Journal of Science 274, 321-355.
1163 Molli, G., 2008. Northern Apennine-Corsica orogenic system: an updated review. In: Siegesmund, S.,
1164 Fugenschuh, B., Froitzheim, N. (Eds.), Tectonic aspects of the Alpine- Dinaride-Carpathian System,
1165 Geological Society of London Special Publication 298, 413-442.
1166 Molli, G., Malavieille, J., 2011. Orogenic processes and the Corsica/Apennine geodynamic
1167 evolution: insights from Taiwan. International Journal of Earth Sciences 100. 1207-1224.
1168 Morillon, A.C., Féraud, G., Sosson, M., Ruffet, G., Crevola, G., Lerouge, G., 2000. Diachronous cooling
1169 on both sides of a major strike slip fault in the Variscan Maures Massif (south-east France), as
1170 deduced from a detailed $^{40}Ar/^{39}Ar$ study. Tectonophysics 321, 103-126.
1171 Morimoto, N., 1988. Nomenclature of pyroxenes. Mineralogy and Petrology 39, 55-76.
1172 Morra, V., Secchi, F.A., Assorgia, A., 1994. Petrogenetic significance of peralkaline rocks from
1173 Cenozoic calc-alkaline volcanism from SW Sardinia, Italy. Chemical Geology 118, 109-142.
1174 Morra, V., Secchi, F.A.G., Melluso, L., Franciosi, L., 1997. High-Mg subduction-related tertiary basalts
1175 in Sardinia, Italy. Lithos 40, 69-91.
1176 Moyen, J.F., 2009. High Sr/Y and La/Yb ratios: the meaning of the "adakitic signature". Lithos 112,
1177 556-574.
1178 Ottaviani-Spella, M.M., Girard, M., Cheilletz, A., 1996. Les ignimbrites burdigaliennes du Sud de la
1179 Corse. Pétrologie et datation K-Ar. Comptes Rendus de l'Académie des Sciences, Série 2, 323, 771-
1180 778.
1181 Ottaviani-Spella, M.M., Girard, M., Rochette, P., Cheilletz, A., Thinon, M., 2001. Le volcanisme acide
1182 Burdigalien du Sud de la Corse: petrologie, datation K-Ar, paleomagnetism. Comptes Rendus de
1183 l'Académie des Sciences de Paris 333, 113-120.

1184 Panza, G., Raykova, R.B., Carminati, E., Doglioni, C., 2007. Upper mantle flow in the western
1185 Mediterranean. Earth and Planetary Science Letters 257, 200-214.
1186 Peacock, S.M., Rushmer, T., Thompson, A.B., 1994. Partial melting of subducting oceaniccrust. Earth
1187 and Planetary Science Letters 121, 227-244.
1188 Peccerillo, A., Poli, G., Serri, G., 1988. Petrogenesis of orenditic and kamafugitic rocks from Central
1189 Italy. Canadian Mineralogist 26, 45-65.
1190 Plank, T., 2014. The chemical composition of subducting sediments.Treatise on Geochemistry 4, 607-
1191 629.
1192 Putirka, K.D., 2008. Thermometers and barometers for volcanic systems. In: Putirka, K.D and Tepley, F.
1193 (Eds.) Minerals, Inclusions and volcanic processes. Reviews in Mineralogy and Geochemistry 69,
1194 61-120.
1195 Rapp, R., Xiao, L., Shimizu, N., 2002. Experimental constraints on the origin of potassium-rich adakites
1196 in eastern China. Acta Petrologica Sinica 18, 293-302.
1197 Réhault, J.P., Honthaas, C., Guennoc, P., Bellon, H., Ruffet, G., Cotten, J., Sosson, M., Maury, R.C.,
1198 2012. Offshore Oligo-Miocene volcanic fields within the Corsica-Liguria Basin: Magmatic diversity
1199 and slab evolution in the western Mediterranean Sea. Journal of Geodynamics 58, 73-95.
1200 Ribeiro, J.M., Maury, R.C., Grégoire, M., 2016. Are adakites slab melts or high-pressure fractionated
1201 mantle melts? Journal of Petrology 57, 839-862.
1202 Rollet, N., Déverchere, J., Beslier, M.O., Guennoc, P., Réhault, J.P., Sosson, M., Truffert, C., 2002. Back
1203 arc extension, tectonic inheritance, and volcanism in the Ligurian Sea, Western Mediterranean.
1204 Tectonics 21, doi:10.1029/2001TC900027.
1205 Rosenbaum, G., 2014. Geodynamics of oroclinal bending; insights from the Mediterranean. Journal of
1206 Geodynamics 82, 5-15.
1207 Rosenbaum, G., Lister, G.S., Duboz, C., 2002. Reconstruction of the tectonic evolution of the western
1208 Mediterranean since the Oligocene. Journal of the Virtual Explorer 8, 107-130.

1209 Rosenbaum, G., Lister, G.S., 2005. The Western Alps from the Jurassic to Oligocene: spatio-temporal
1210 constraints and evolutionary reconstructions. Earth-Science Reviews 69, 281-306.
1211 Rosenberg, C.L., 2004. Shear zones and magma ascent: a model based on a review of the Tertiary
1212 magmatism in the Alps. Tectonics 23, doi:10.1029/2003TC001526
1213 Sajona, F.G., Bellon, H., Maury, R.C., Cotten, J., Defant, M.J., Pubellier, M., 1993. Initiation of
1214 subduction and the generation of slab melts in western and eastern Mindanao, Philippines. Geology
1215 21, 1007-1010.
1216 Sajona, F.G., Bellon, H., Maury, R., Pubellier, M., Cotten, J., Rangin, C., 1994. Magmatic response to
1217 abrupt changes in geodynamic settings: Pliocene-Quaternary calc-alkaline and Nb-enriched lavas
1218 from Mindanao (Philippines). Tectonophysics 237, 47-72.
1219 Sartori, R., 1990. The main results of ODP Leg 107 in the frame of Neogene to Recent geology of
1220 Perityrrhenian areas. Procedings of the Ocean Drilling Program Scientific Results 107, 715-730.
1221 Séranne, M., Benedicto, A., Labaum, P., Truffert, C., Pascal, G., 1995. Structural style and evolution of
1222 the Gulf of Lion Oligo-Miocene rifting: Role of the Pyrenean orogeny. Marine and Petroleum
1223 Geology 12, 809-820.
1224 Schmid, C., Van Der Lee, S., Van Decar, J.C., Engdahl, E.R., Giardini, D., 2008. Three-dimensional S
1225 velocity of the mantle in the Africa-Eurasia plate boundary region from phase arrival times and
1226 regional waveforms. Journal of Geophysical Research Solid Earth 113(B3).
1227 Stampfli, G.M., Borel, G.D., 2002. A plate tectonic model for the Paleozoic and Mesozoic constrained
1228 by dynamic plate boundaries and restored synthetic oceanic isochrons. Earth and Planetary Science
1229 Letters 196, 17-33.
1230 Stracke, A., 2012. Earth's heterogeneous mantle: a product of convection-driven interaction between
1231 crust and mantle. Chemical Geology 330, 274-299.
1232 Terrier, M., Serrano, O., Hanot, F., 2008. Reassessment of the structural framework of western Provence
1233 (France): consequence on the regional seismotectonic model. Geodinamica Acta 21, 231-238.

1234 Thorkelson, D.J., 1996. Subduction of diverging plates and the principles of slab window formation.
1235 Tectonophysics 255, 47-63.
1236 Torsvik, T.H., Cocks, L.R.M., 2004. Earth geography from 400 to 250 Ma: a palaeomagnetic, faunal
1237 and facies. Journal of the Geological Society of London 161, 555-572.
1238 Turco, E., Macchiavelli, C., Mazzoli, S., Schettino, A., Pierantoni, P.P., 2012. Kinematic
1239 evolution of Alpine Corsica in the framework of Mediterranean mountain belt.
1240 Tectonophysics 579, 193-206.
1241 Turner, S.P., Platt, J.P., George, R.M.M., Kelley, S.P., Pearson, D.G., Nowell, G.M., 1999. Magmatism
1242 associated with orogenic collapse of the Betic-Alborán domain southeast Spain. Journal of Petrology
1243 40, 1011-1036.
1244 von Blanckenburg, F., Davies, J.H., 1995. Slab breakoff: a model for syncollisional magmatism and
1245 tectonics in the Alps. Tectonics 14, 120-131.
1246 Wang, Q., Xu, J.-F., Jian, P., Bao Z.-W., Zhao, Z.-H., Li, C.-F., Xiong, X.-L., Ma, J.-L., 2006.
1247 Petrogenesis of adakitic porphyries in an extensional tectonic setting, Dexing, South China:
1248 implications for the genesis of Porphyry Copper mineralization. Journal of Petrology 47, 119-144.
1249 Wang, Q., Wyman, D.A., Xu, J., Wan, Y., Li, C., Zi, F., Dong, Y., 2007a. Triassic Nb-enriched basalts,
1250 magnesian andesites, and adakites of the Qiangtang terrane (Central Tibet): evidence for
1251 metasomatism by slab derived melts in the mantle wedge. Contributions to Mineralogy and
1252 Petrology 155, 473-490.
1253 Wang, Q., Wyman, D.A., Zhao, Z.H., Xu, J.F., Bai, Z. H., Xiong, X.L., Chu, Z.Y., 2007b. Petrogenesis
1254 of carboniferous adakites and Nb-enriched arc basalts in the Alataw area, northern Tianshan Range
1255 (western China): implications for Phanerozoic crustal growth in the central Asia orogenic belt.
1256 Chemical Geology 236, 42-64.

1257 Waters, L.E., Lange, R.A., 2015. An updated calibration of the plagioclase-liquid hygrometer-
1258 thermometer applicable to basalts through rhyolites. American Mineralogist 100, 2172-
1259 2184.
1260 Weil, A.B., Gutiérrez-Alonso, G., Johnston, S.T., Pastor-Galán, D., 2013. Kinematic constraints on
1261 buckling a lithospheric-scale orocline along the northern margin of Gondwana: A geologic synthesis.
1262 Tectonophysics 582, 25-49.
1263 Willbold, M., Stracke, A., 2006. Trace element composition of mantle end-members: Implications for
1264 recycling of oceanic and upper and lower continental crust. Geochemistry Geophysics Geosystems 7,
1265 doi.org/10.1029/2005GC001005
1266 Xu, Y.G., Huang, X.L., Ma, J.L., Wang, Y.B., Iizuka, Y., Xu, J.F., Wu, X.Y., 2004. Crust–mantle
1267 interaction during the tectono-thermal reactivation of the North China craton: constraints from
1268 SHRIMP U-Pb zircon chronology and geochemistry of Mesozoic plutons from Western Shandong.
1269 Contributions to Mineralogy and Petrology 147, 750-767.
1270 Ziegler, P.A., Dèzes, P., 2007. Cenozoic uplift of Variscan Massifs in the Alpine foreland: timing and
1271 controlling mechanisms. Global Planet Change 58, 237-269.
1272 Zhou, M.F., Yan, D.P., Wang, C.L., Qi, L., Kennedy, A., 2006. Subduction-related origin of the 750 Ma
1273 Xuelongbao adakitic complex (Sichuan Province, China): implications for the tectonic setting of the
1274 giant Neoproterozoic magmatic event in South China. Earth and Planetary Science Letters 248, 286-
1275 300.
1276 Ziberna, L., Klemme, S., Nimis, P., 2013. Garnet and spinel in fertile and depleted mantle: insights from
1277 thermodynamic modelling. Contributions to Mineralogy and Petrology 166, 411-421,
1278 doi:10.1007/s00410-013-0882-5.
1279

Figure captions

Fig. 1. Geological schetch map of Provence (modified from BRGM Geological Map of France 1:250000) with locations of collected LEEM and LMP Cenozoic igneous rock samples. MDF: Mid-Durance Fault System; AF: Aix-en-Provence Fault.

Fig. 2. Crossed polarizers photomicrographs for selected representative rock samples from the two Cenozoic igneous cycles of Provence (LEEM and LMP). **a)** LEEM basaltic andesite sample FEM7 showing a porphyritic texture with more abundant plagioclase and lesser clinopyroxene phenocrysts (tabular crystals at the centre, with high interference colours) set within a hypocrystalline groundmass; **b)** LEEM andesite sample FEM20 showing the typical porphyritic texture dominated by plagioclase phenocrysts; **c)** LEEM dacite sample FEM9 with a porphyritic texture dominated by plagioclase phenocrysts; **d)** LMP basalt sample FEM33 with the characteristic aphyric texture with sporadic olivine microphenocrysts (e.g., lower right) set within a hypocrystalline groundmass.

Fig. 3. Composition of the analysed **a)** feldspar and **b)** pyroxene crystals from the rocks of the two Cenozoic igneous cycles of Provence (LEEM and LMP).

Fig. 4. Age release, radiogenic Ar content and K/Ca spectra for plagioclase and groundmass concentrates from five representative samples from the two Cenozoic igneous cycles of Provence (LEEM and LMP).

Fig. 5. TAS classification diagram (LeMaitre, 2002) for whole-rock compositions for the two Cenozoic igneous cycles of Provence (LEEM and LMP). Also shown are the literature data for coeval Cenozoic "orogenic" and "anorogenic" rocks from Sardinia, Spain, Corsica-Estérel, Languedoc, Northern Apennines and Alps (see ESM1 for bibliographic sources). The dotted line separates the fields for subalkaline and alkaline rock series (Irvine and Baragar, 1971).

Fig. 6. **a)** K_2O vs. SiO_2 (modified after Le Maitre, 2002) and **b)** FeO*/MgO vs. SiO_2 diagrams for the rocks of the two Cenozoic igneous cycles of Provence (LEEM and LMP). Symbols and literature data as in Fig. 5. In b) the thick black lines separate high-Fe, medium-Fe and low-Fe series according to Arculus (2003), whereas the gray dashed line separates tholeiitic and calcalkaline series after Miyashiro (1974).

Fig. 7. Selected major element binary variation diagrams for the rocks of the two Cenozoic igneous cycles of Provence (LEEM and LMP). Symbols and literature data as in Fig. 5.

Fig. 8. Selected trace element binary variation diagrams for the rocks of the two Cenozoic igneous cycles of Provence (LEEM and LMP). Symbols and literature data as in Fig. 5.

Fig. 9. Primitive-mantle normalized diagram [after Lyubetskaya and Korenaga (2007)] for the **a)** LEEM and **b)** LMP Cenozoic igneous rocks from Provence. The estimated composition of global subducted sediments (GLOSS-II; Plank, 2014) and the field for the typical HiMu-OIB locality (*high-μ*, i.e., high $^{238}U/^{204}Pb$, Ocean Island Basalt from St. Helena Island, Southern Atlantic Ocean; Kawabata et al., 2011 and references therein) are reported for comparison.

Fig. 10. **a)** $^{143}Nd/^{144}Nd$ vs. $^{87}Sr/^{86}Sr$, **b)** $^{207}Pb/^{204}Pb$ vs. $^{206}Pb/^{204}Pb$, **c)** $^{208}Pb/^{204}Pb$ vs. $^{206}Pb/^{204}Pb$ and **d)** $^{207}Pb/^{206}Pb$ vs. $^{208}Pb/^{206}Pb$ diagrams for the rocks of the two Cenozoic igneous cycles of Provence (LEEM and LMP). Symbols and literature data as in Fig. 5. Also shown are the isotopic compositions for BSE (Bulk Silicate Earth) and ChUR (Chondritic Uniform Reservoir), the DMM (Depleted MORB Mantle), HiMu-OIB (*high-μ* Ocean Island Basalt) and EM-I and EM-II (Enriched Mantle I and II) mantle end-members, the 4.56 Ga Geochron and the Northern Hemisphere Reference Line (NHRL).

Fig. 11. **a)** $^{206}Pb/^{204}Pb$ vs. $^{87}Sr/^{86}Sr$, **b)** $^{207}Pb/^{204}Pb$ vs. $^{87}Sr/^{86}Sr$ and **c)** $^{208}Pb/^{204}Pb$ vs. $^{87}Sr/^{86}Sr$ diagrams for the rocks of the two Cenozoic igneous cycles of Provence (LEEM and LMP). Symbols and literature data as in Fig. 5.

Fig. 12. **a)** Mg# in clinopyroxene vs. Mg# whole rock and **b)** CaO/Na_2O in plagioclase vs. CaO/Na_2O in whole rock diagrams for the rocks of the two Cenozoic igneous cycles of Provence (LEEM and LMP). The equilibrium curves for $K_D(Fe\text{-}Mg)^{cpx/melt} = 0.27\pm0.03$ and for different values of $K_D(Ca\text{-}Na)^{pl/melt}$ [with respective H_2O contents in the melt, according to Martel et al. (2006)] are also shown.

Table captions

Table 1. Results of laser step-heating $^{40}Ar/^{39}Ar$ dating for the rocks of the two Cenozoic igneous cycles (LEEM and LMP) of Provence. Rock type: A = andesitic; D = dacitic; B = basalt.

Table 2. Major- and trace element concentrations (respectively in wt.% recalculated to 100% water-free, and in ppm) and age-corrected Sr-Nd-Pb isotope ratios for some representative rock samples from the two Cenozoic igneous cycles (LEEM and LMP) of Provence. Rock type: A = andesitic; D = dacitic; B = basalt. LOI = (mass) loss on ignition (wt.%); Mg# = molar $Mg/(Fe^{2+}+Mg+Mn)$; bdl = below detection limit.

Figures

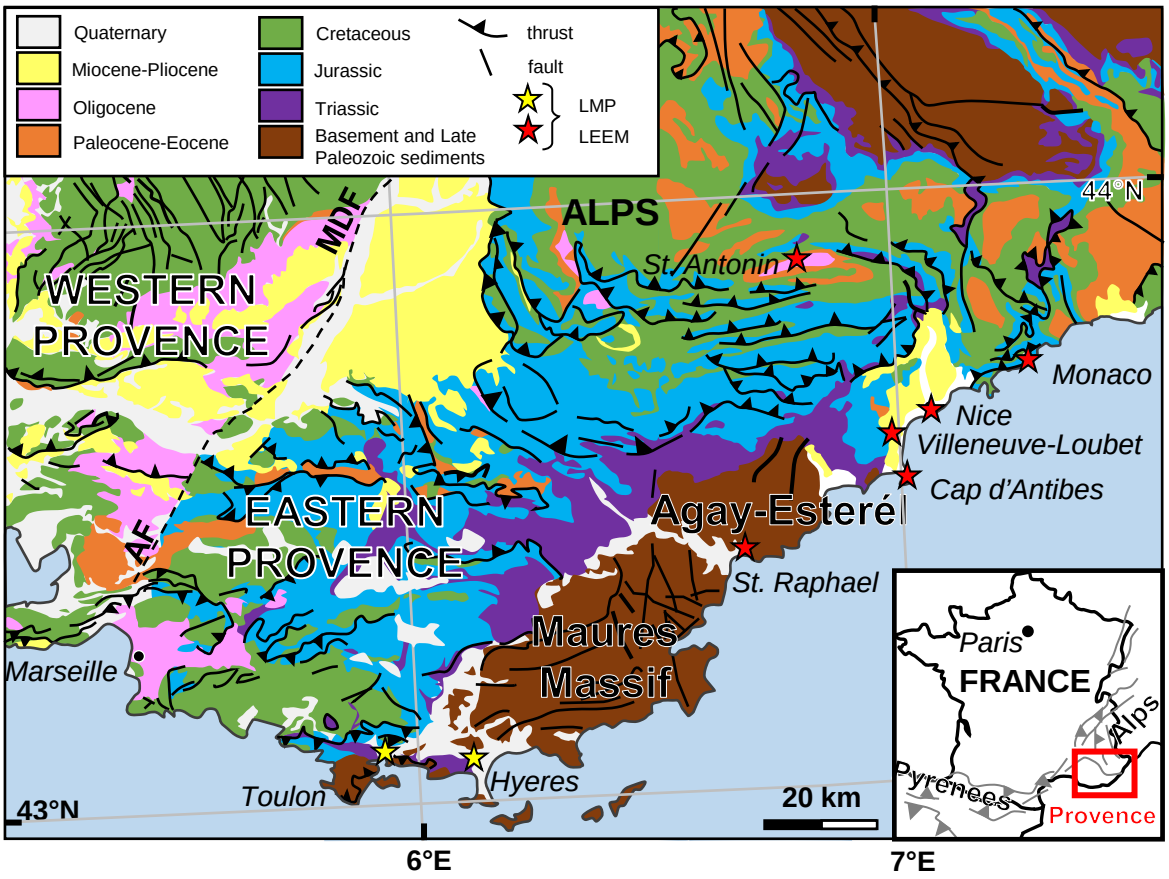

Fig. 1 (Lustrino et al. – Lithos)

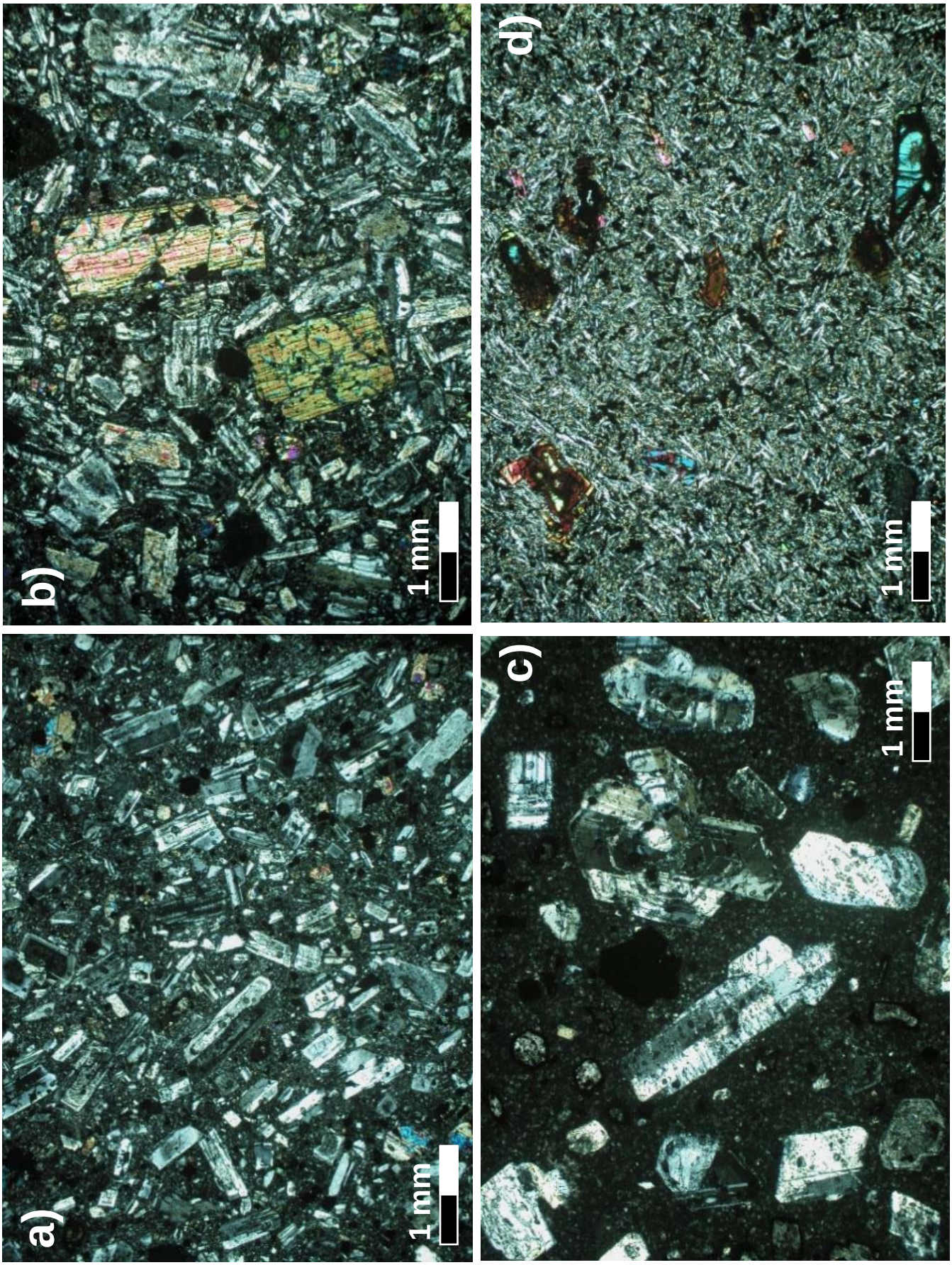

Fig. 2 (Lustrino et al. – Lithos)

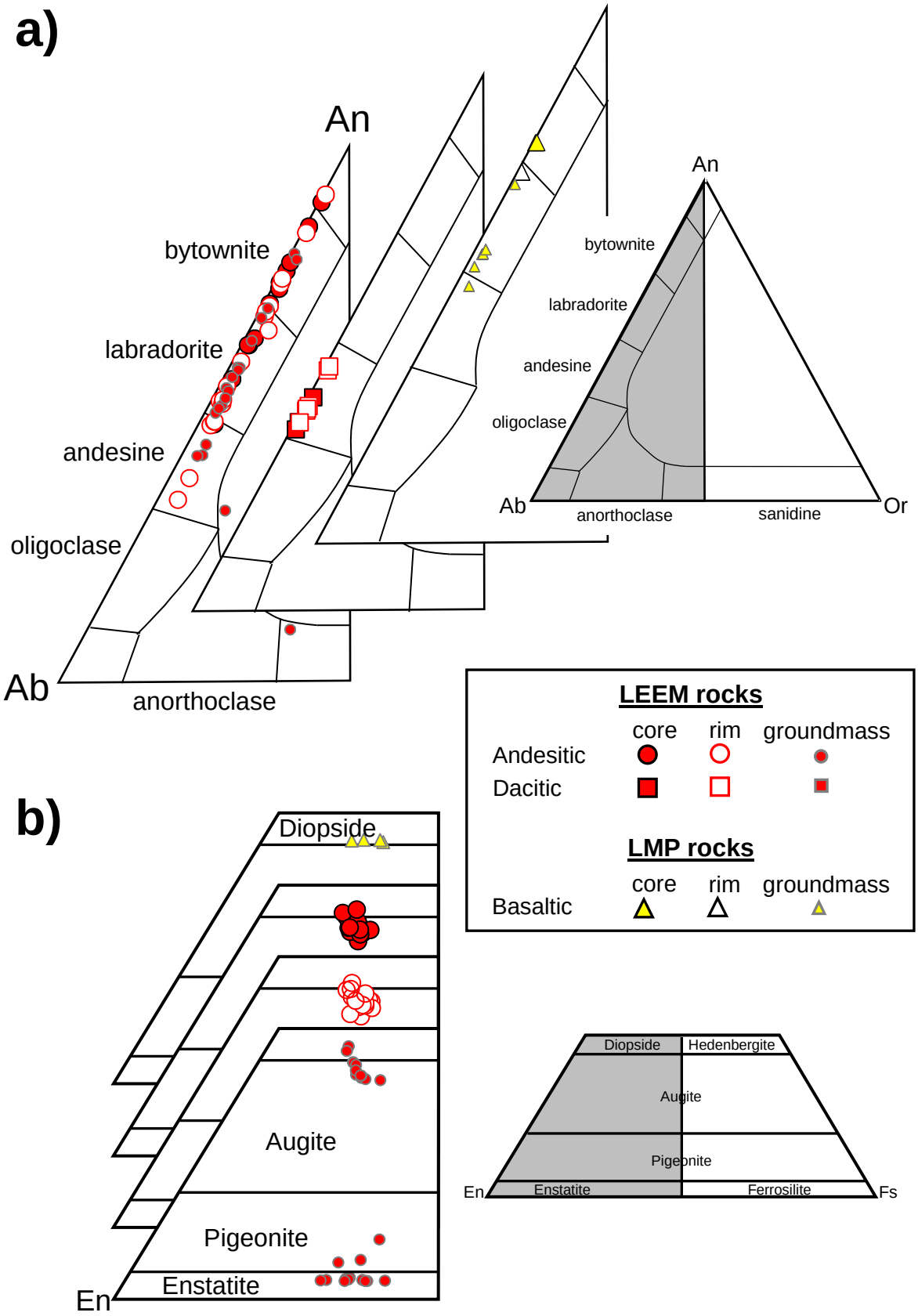

Fig. 3 (Lustrino et al. – Lithos)

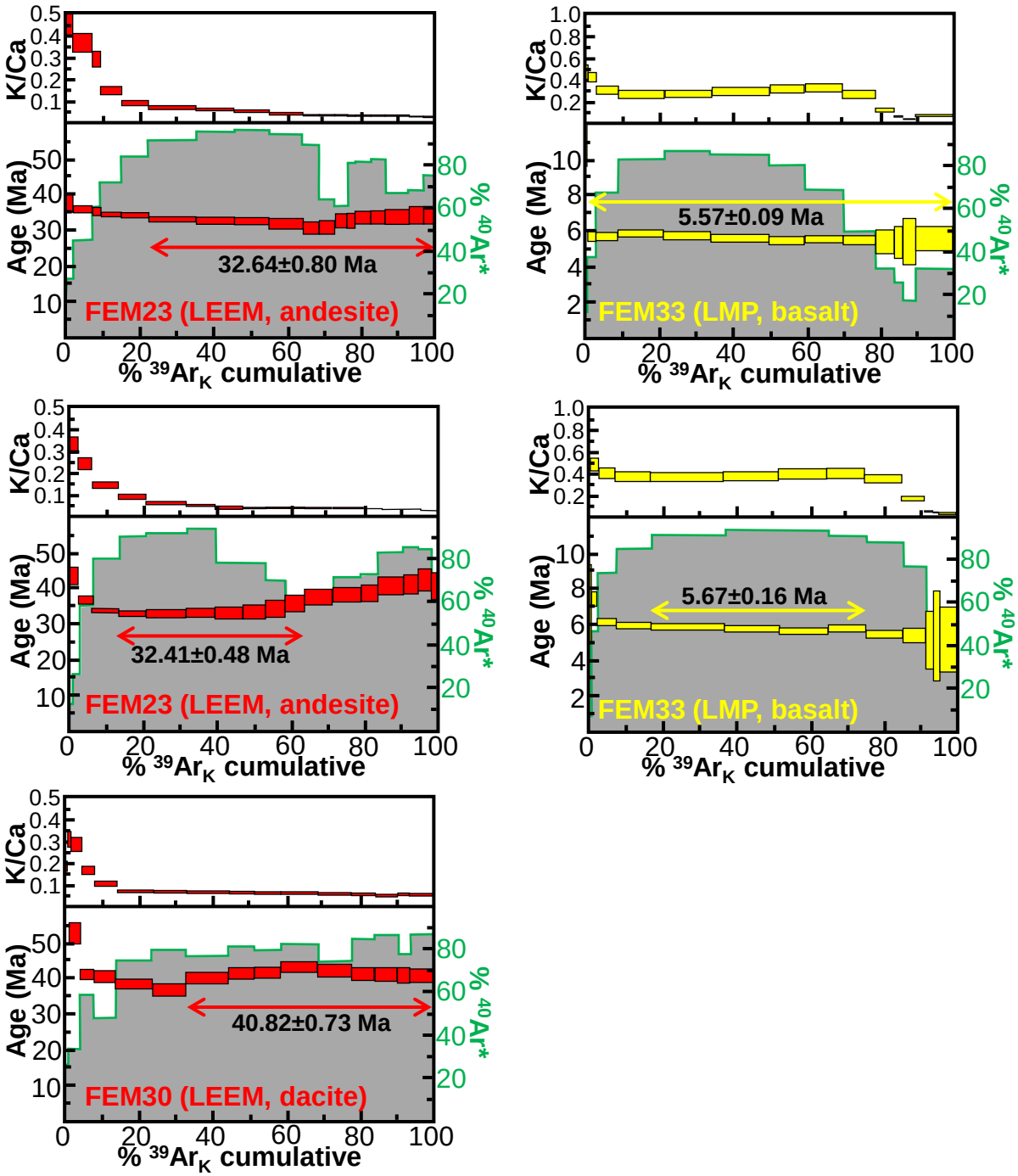

Fig. 4 (Lustrino et al. – Lithos)

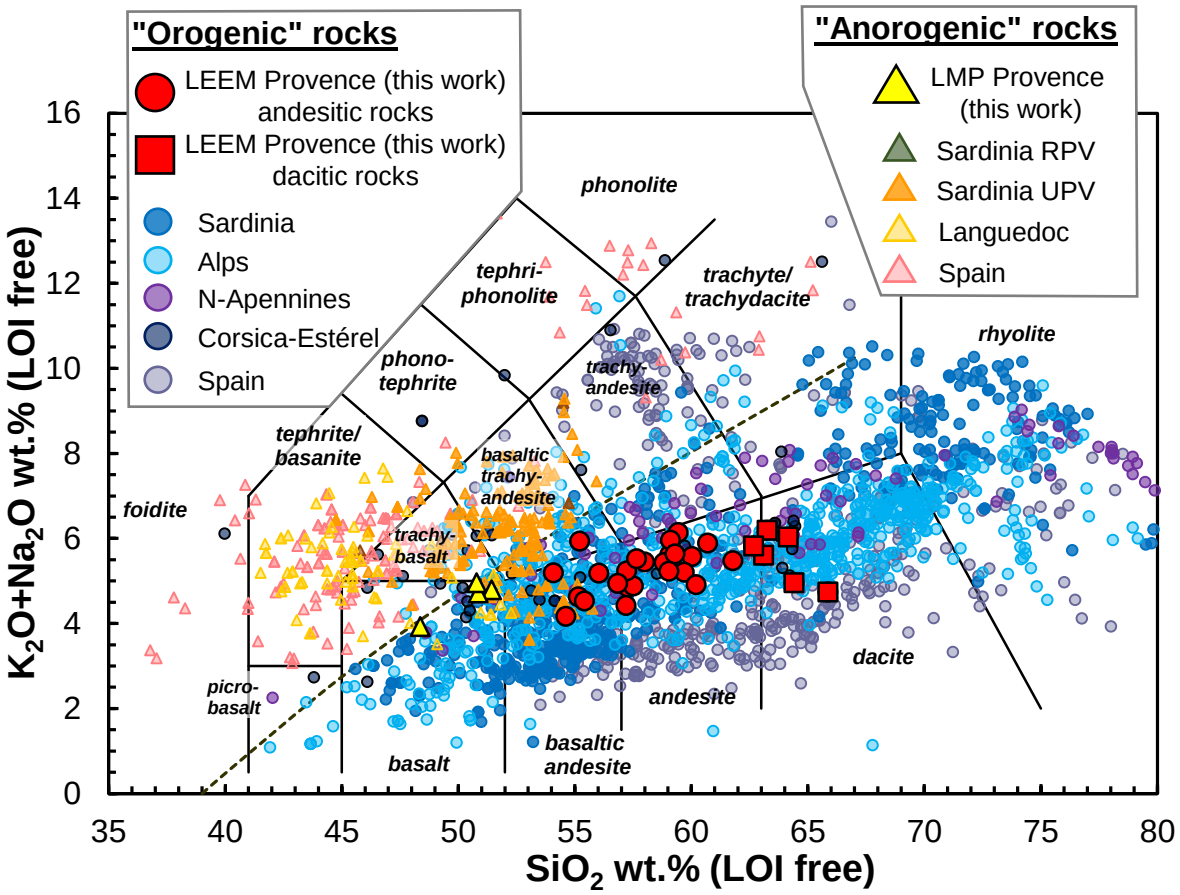

Fig. 5 (Lustrino et al. – Lithos)

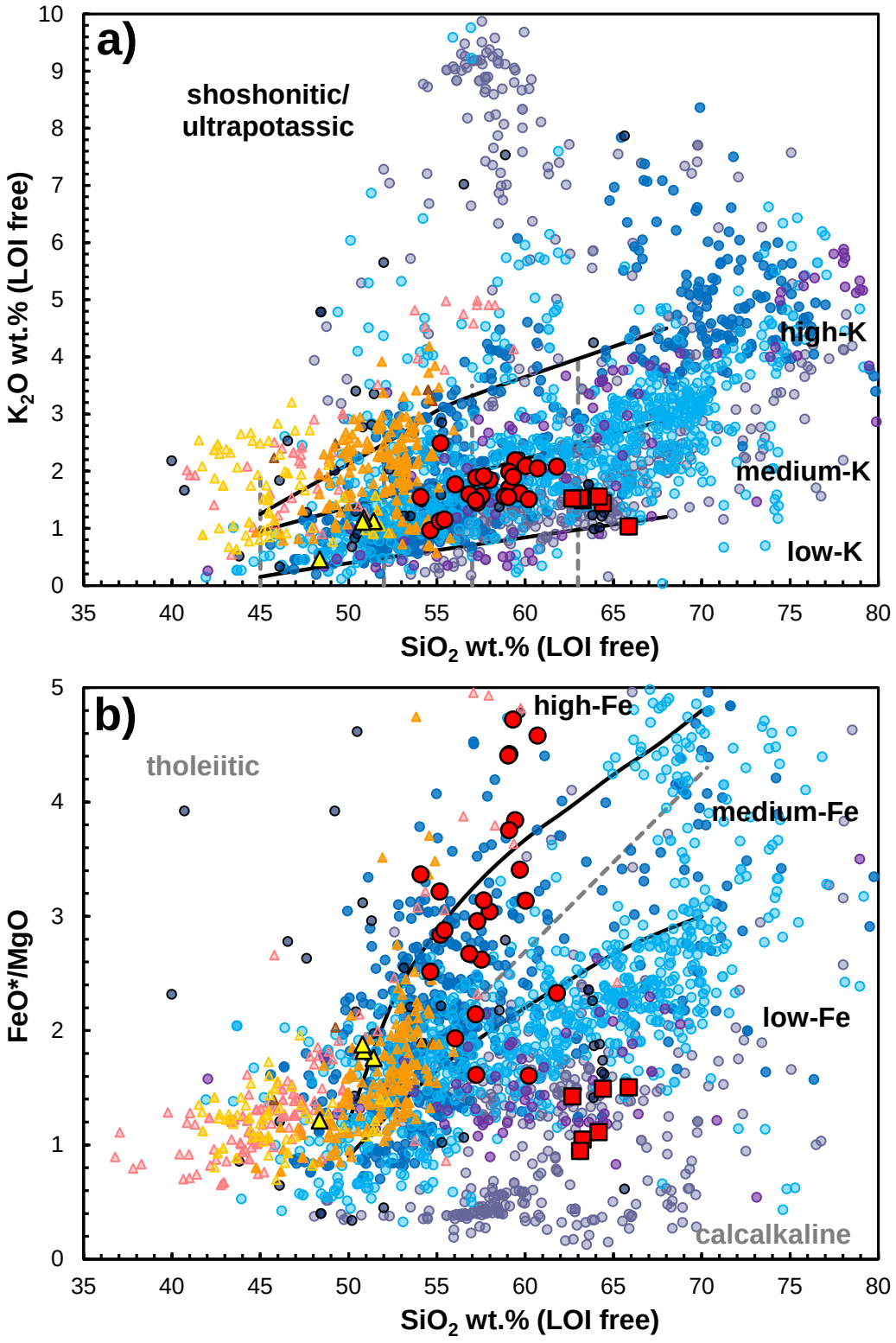

Fig. 6 (Lustrino et al. – Lithos)

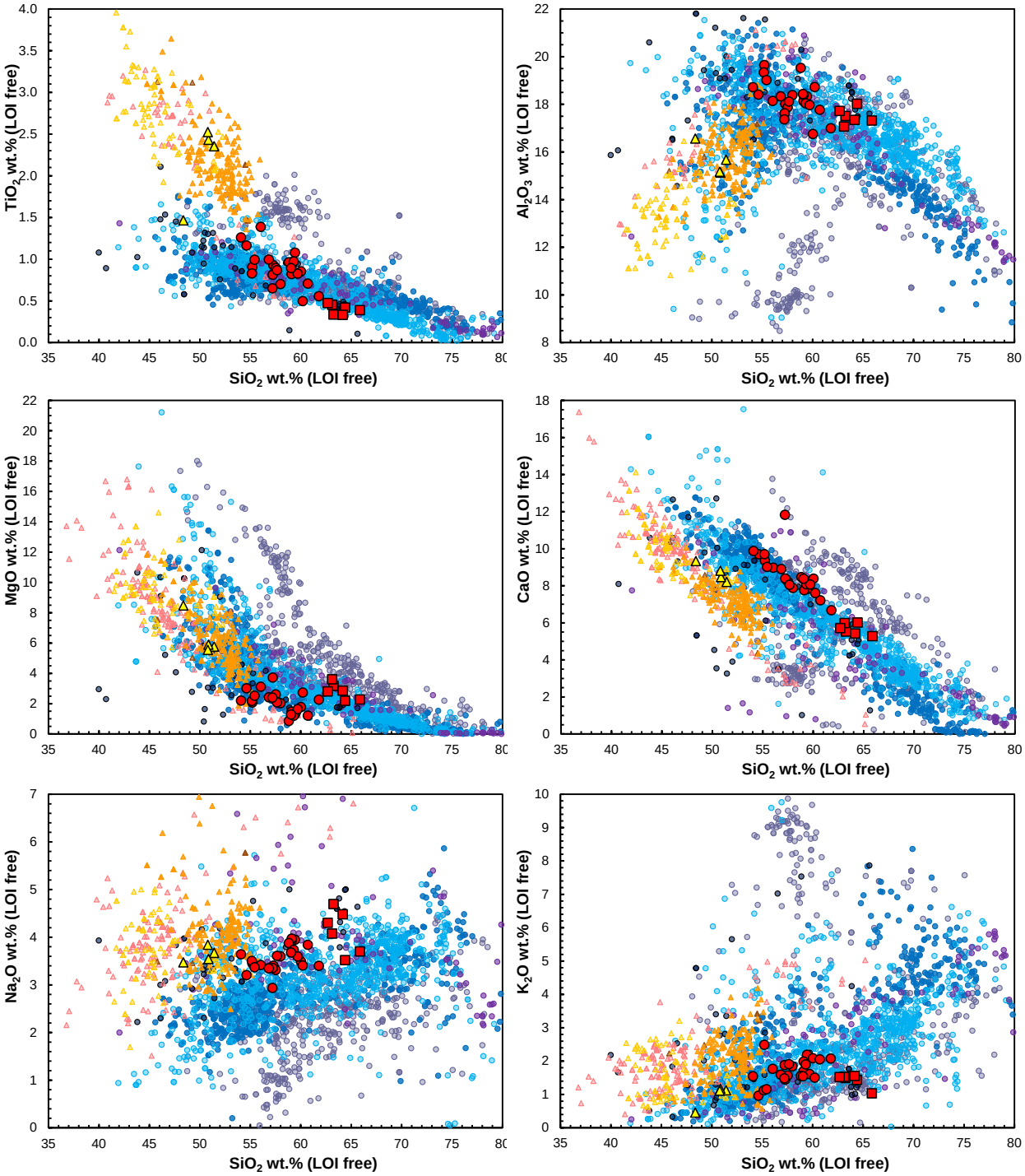

Fig. 7 (Lustrino et al. – Lithos)

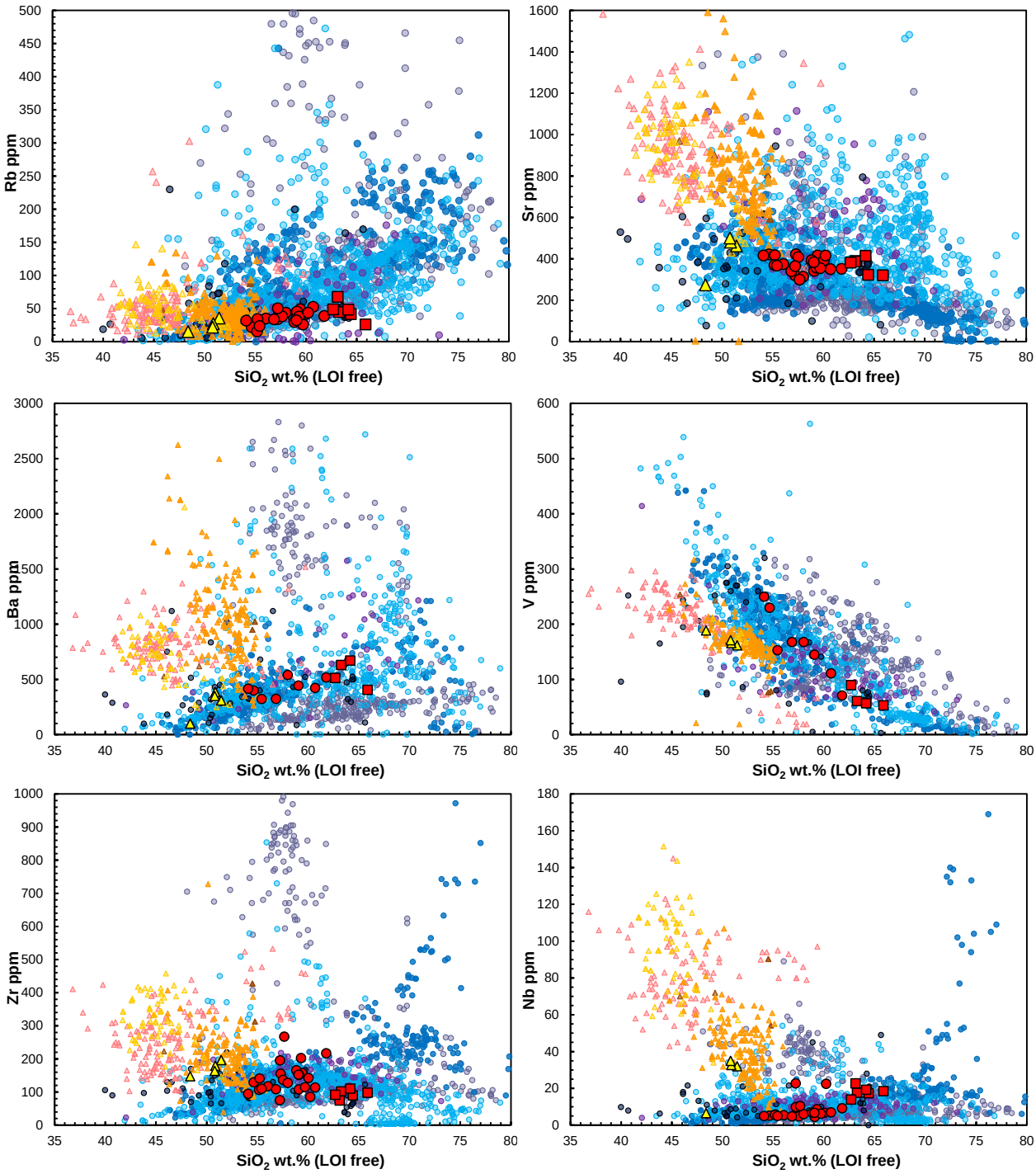

Fig. 8 (Lustrino et al. – Lithos)

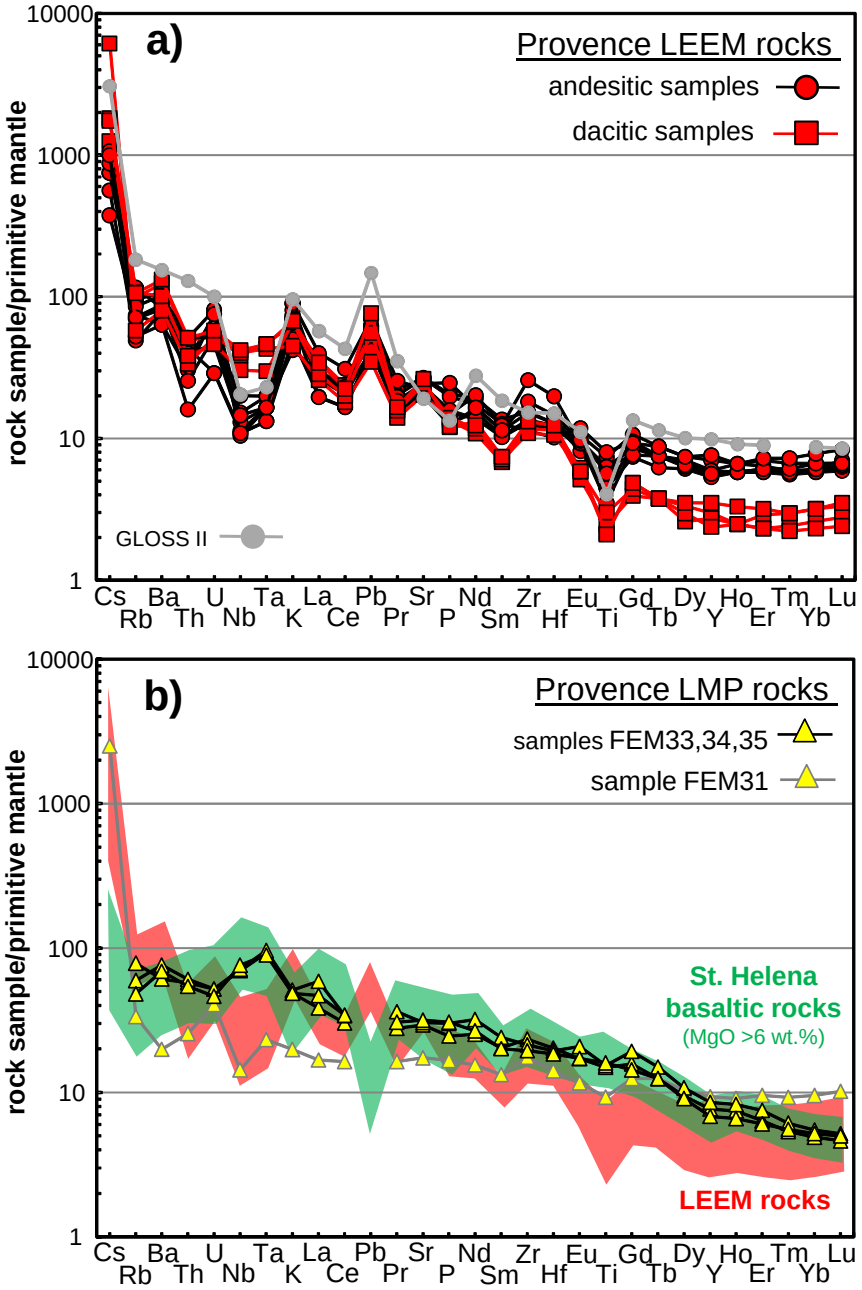

Fig. 9 (Lustrino et al. – Lithos)

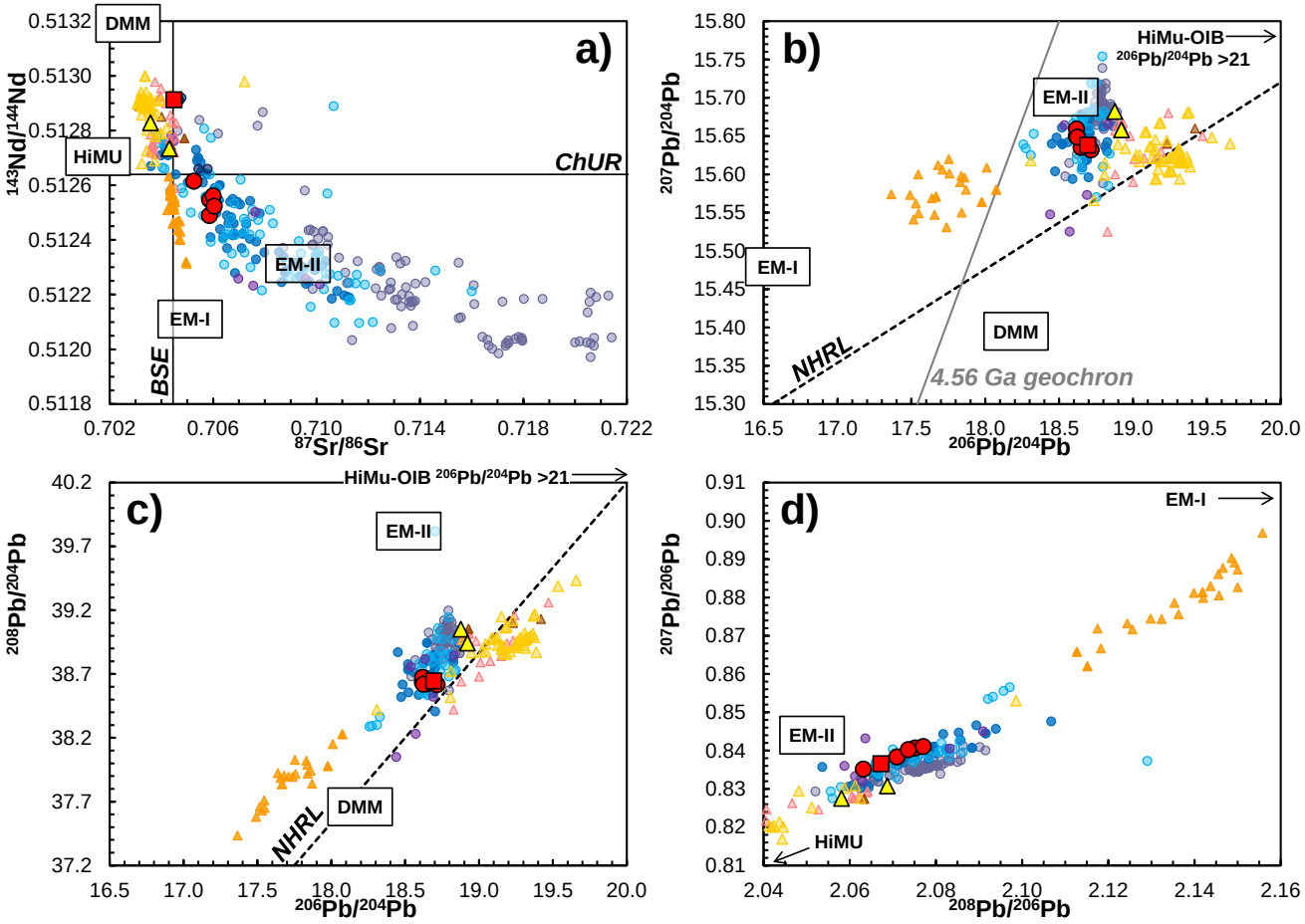

Fig. 10 (Lustrino et al. – Lithos)

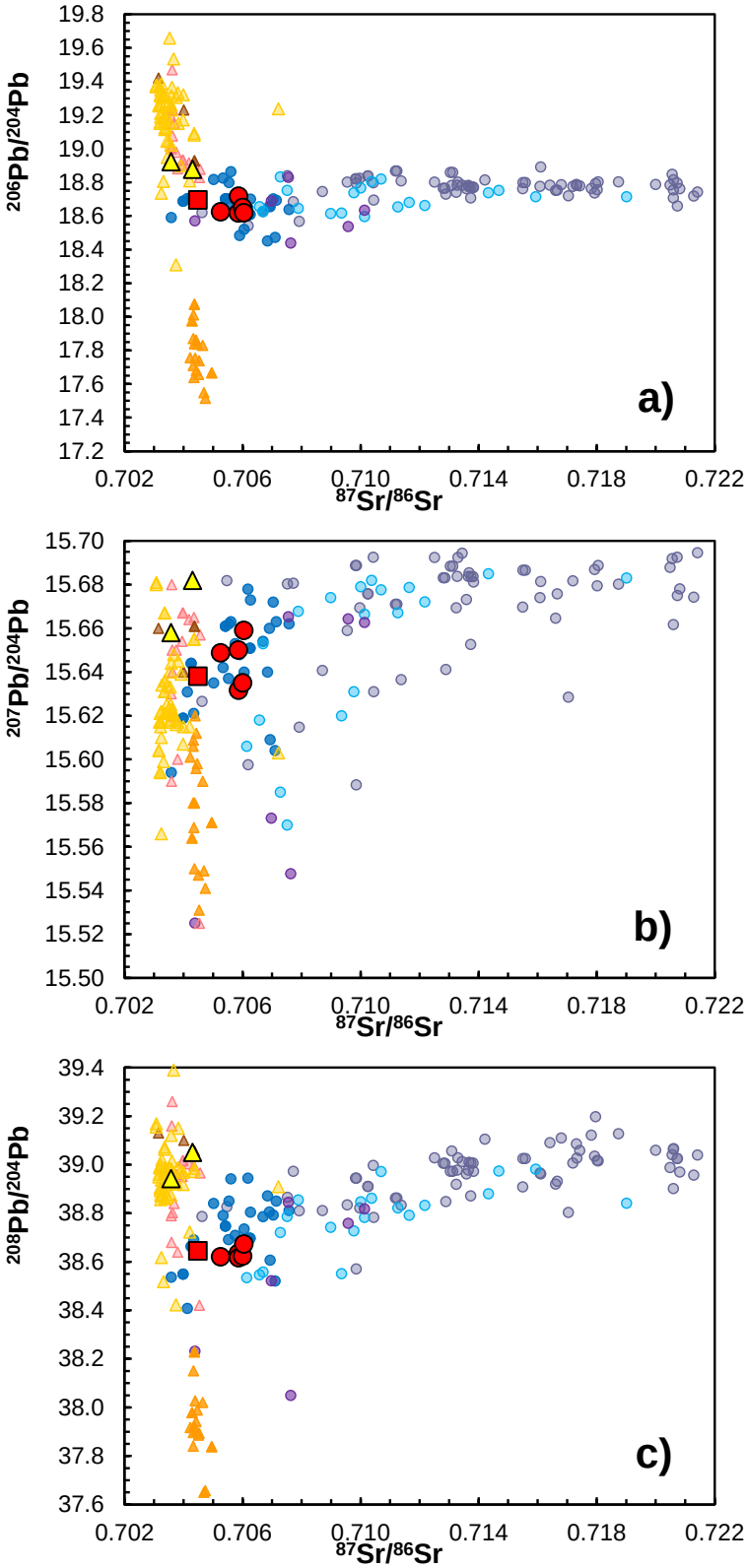

Fig. 11 (Lustrino et al. – Lithos)

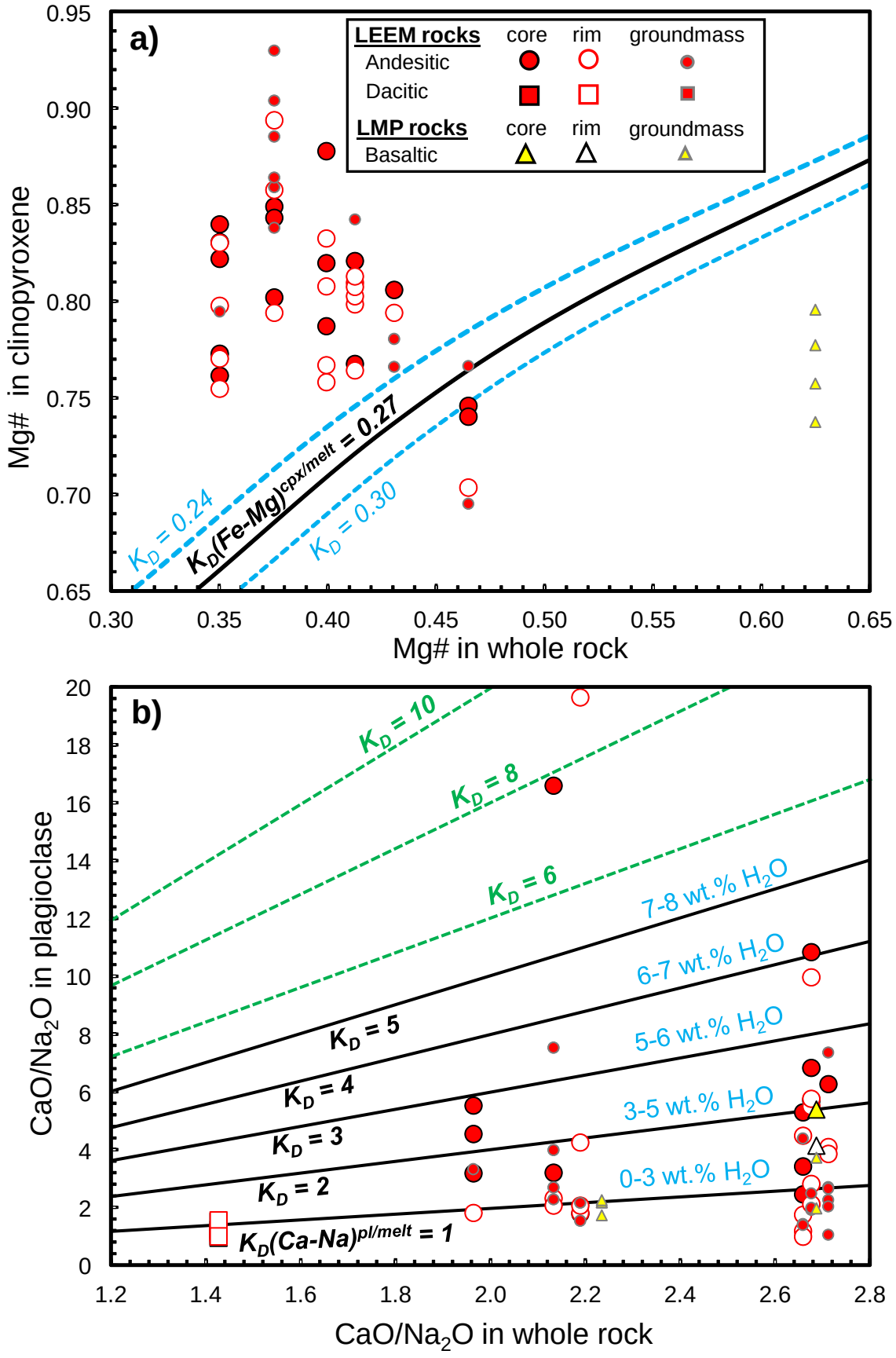

Fig. 12 (Lustrino et al. – Lithos)

Tables

Click here to download Table: FEM (Tables).xlsx

Sample	cycle	rock	material analyzed	Total gas age (Ma)	±2σ (internal error)	Error-weighted mean age on concordant segment (Ma)	±2σ (internal error)	probability	consecuitve steps included in the calculation	$^{39}Ar_K$ %	age from isochron plot (Ma)	±2σ (internal error)	$(^{40}Ar/^{36}Ar)_i$	±2σ	probability	consecutive steps included in the calculation	$^{39}Ar_K$ %	**preferred age (Ma)**	**±2σ (internal error)**
FEM4	LEEM	A	plagioclase	33.09	0.40	32.64	0.80	0.13	13/20 (8 to 20)	77.6	32.47	0.78	305	30	0.11	13/20 (8 to 20)	77.6	**32.47**	**0.78**
FEM23	LEEM	A	plagioclase	35.23	0.52	32.41	0.48	0.37	7/18 (5 to 11)	50.5	31.48	0.70	351	18	0.32	9/18 (5 to 13)	65.9	**31.40**	**0.84**
FEM30	LEEM	D	plagioclase	46.56	0.58	40.82	0.73	0.24	9/17 (8 to 16)	66.8	39.3	2.7	339	75	0.28	9/17 (8 to 16)	66.8	**40.82**	**0.73**
FEM33	LMP	B	groundmass	5.59	0.12	5.574	0.093	0.13	12/14 (3 to 14)	99.1	5.59	0.13	294	9.8	0.093	12/14 (3 to 14)	99.1	**5.574**	**0.093**
FEM35	LMP	B	groundmass	5.65	0.12	5.67	0.16	0.12	4/13 (5 to 8)	58.4	5.47	0.25	429	130	0.72	5/13 (4 to 8)	67.8	**5.67**	**0.16**

Electronic Supplementary Material 1

Click here to download Background dataset for online publication only: FEM (Electronic Supplementary Material - 1).docx

Electronic Supplementary Material 2

Click here to download Background dataset for online publication only: FEM (Electronic Supplementary Material - 2).xlsx

Electronic Supplementary Material 3-4-5-6

Click here to download Background dataset for online publication only: FEM (Electronic Supplementary Material 3-4-5-6).pdf